

E 201 241

2

AD-A258 602



PL-TR-92-2112

**ANALYSIS OF SOLAR TRANSMISSION DATA
FROM SABLE 89**

D.R. Longtin

SPARTA, Inc.
24 Hartwell Avenue
Lexington, MA 02173

S DTIC ELECTE D
OCT 0 8 1992
A

1 May 1992

Scientific Report No. 2

Approved for public release; distribution unlimited

92-26672



**PHILLIPS LABORATORY
AIR FORCE SYSTEMS COMMAND
HANSCOM AIR FORCE BASE, MASSACHUSETTS 01731-5000**

92 10 7 029

This technical report has been reviewed and is approved for publication.


(signature)
MARK A. CLOUTIER, Capt., USAF
Contract Manager


(signature)
DONALD E. BEDO, Branch Chief
Electro-Optical Measurements


(Signature)
ALAN D. BLACKBURN, Col., USAF
Director, Optical Environment Division

This document has been reviewed by the ESD Public Affairs Office (PA) and is releasable to the National Technical Information Service (NTIS).

Qualified requestors may obtain additional copies from the Defense Technical Information Center. All others should apply to the National Technical Information Service.

If your address has changed, or if you wish to be removed from the mailing list, or if the addressee is no longer employed by your organization, please notify PL/TSI, Hanscom AFB, MA 01731-5000. This will assist us in maintaining a current mailing list.

Do not return copies of this report unless contractual obligations or notices on a specific document requires that it be returned.

| REPORT DOCUMENTATION PAGE | | | Form Approved OMB No. 0704-0188 | |
|--|---|--|--|--|
| Public reporting burden for this collection of information is estimated to average 1 hour per response, including the time for reviewing instructions, searching existing data sources, gathering and maintaining the data needed, and completing and reviewing the collection of information. Send comments regarding this burden estimate or any other aspect of this collection of information, including suggestions for reducing this burden, to Washington Headquarters Services, Directorate for Information Operations and Reports, 1215 Jefferson Davis Highway, Suite 1204, Arlington, VA 22202-4302, and to the Office of Management and Budget, Paperwork Reduction Project (0704-0188), Washington, DC 20503. | | | | |
| 1. AGENCY USE ONLY (Leave blank) | | 2. REPORT DATE 01 MAY 1992 | 3. REPORT TYPE AND DATES COVERED SCIENTIFIC REPORT NO. 2 | |
| 4. TITLE AND SUBTITLE ANALYSIS OF SOLAR TRANSMISSION DATA FROM SABLE 89 | | | 5. FUNDING NUMBERS PE35160F PR7670TA15 WUBB Contract-F19628-91-C-0093 | |
| 6. AUTHOR(S) D.R. LONGTIN | | | | |
| 7. PERFORMING ORGANIZATION NAME(S) AND ADDRESS(ES) SPARTA, Inc. 24 Hartwell Avenue Lexington, MA 02173 | | | 8. PERFORMING ORGANIZATION REPORT NUMBER LTR92-005 | |
| 9. SPONSORING / MONITORING AGENCY NAME(S) AND ADDRESS(ES) PHILLIPS LABORATORY HANSCOM AFB, MASSACHUSETTS 01731-5000 Contract Manager: Capt Mark Cloutier/GPOA | | | 10. SPONSORING / MONITORING AGENCY REPORT NUMBER PL-TR-92-2112 | |
| 11. SUPPLEMENTARY NOTES | | | | |
| 12a. DISTRIBUTION / AVAILABILITY STATEMENT APPROVED FOR PUBLIC RELEASE; DISTRIBUTED UNLIMITED | | | 12b. DISTRIBUTION CODE | |
| 13. ABSTRACT (Maximum 200 words) This report analyzes solar transmissometer data that was taken during the South Atlantic Backscatter Lidar Experiment (SABLE). The instrument operated on six days between 25 June and 7 July 1989. The instrument was located on Ascension Island, and it measured solar transmission at 532 nm versus time and transmission across the solar spectrum. Time series of solar transmissions at 532 nm are used to study the properties of cirrus and boundary layer stratocumulus that passed in front of the sun while the instrument was working. For 25 June 1989, a qualitative assessment shows the transmissions through cirrus to be between 0.4 and 0.8, and the cirrus thicknesses are estimated to be between 1.0 and 2.2 km. These estimates are consistent with cirrus observations and from aircraft. The analysis also focuses on the properties of the stratocumulus cloud edges and thin spots. Stratocumulus are shown to have very similar edge characteristics from day-to-day: there is a uniform distribution of cloud transmission values between about 0.1 and 0.7, and the percentages increase significantly as cloud transmissions increase from 0.7 to 0.9. The number of occurrences of stratocumulus thin spots and edges are then compared against the total number of stratocumulus occurrences. The comparisons clearly show that the stratocumulus over Ascension Island often are not optically thick and they frequently transmit partial direct solar radiation. | | | | |
| 14. SUBJECT TERMS SABLE, Solar Transmission, Cloud Opacity, Aerosols, Maritime Environment | | | 15. NUMBER OF PAGES 68 | |
| | | | 16. PRICE CODE | |
| 17. SECURITY CLASSIFICATION OF REPORT Unclassified | 18. SECURITY CLASSIFICATION OF THIS PAGE Unclassified | 19. SECURITY CLASSIFICATION OF ABSTRACT Unclassified | 20. LIMITATION OF ABSTRACT SAR | |

| | |
|--------------------|-------------------------------------|
| Accession For | |
| NTIS CRA&I | <input checked="" type="checkbox"/> |
| DTIC TAB | <input type="checkbox"/> |
| Unannounced | <input type="checkbox"/> |
| Justification | |
| By | |
| Distribution/ | |
| Availability Codes | |
| Dist | Avail and/or Special |
| A-1 | |

Contents

| | | |
|------------|---|----|
| 1 | INTRODUCTION | 1 |
| 1.1 | Purpose and Organization of Report | 1 |
| 2 | VALIDATION OF SOLAR TRANSMISSION MEASUREMENTS | 4 |
| 2.1 | Concerns About Instrument Calibration | 4 |
| 2.2 | Recalibration Using the Langley Method | 4 |
| 3 | ANALYSIS OF SOLAR TRANSMISSOMETER DATA AT 532 nm | 6 |
| 3.1 | Removal Of Aerosol Effects | 15 |
| 3.2 | Discussion of Forward Scattering Effects | 24 |
| 3.3 | Cirrus Cloud Analysis | 25 |
| 3.4 | Stratocumulus Cloud Analysis | 27 |
| 3.4.1 | Thickness Estimates of Cloud Edges and Thin Spots | 27 |
| 3.4.2 | Occurrence of Cloud Edges and Thin Spots | 27 |
| 3.4.3 | Time Duration of Cloud Edges and Thin Spots | 32 |
| 4 | SUMMARY AND CONCLUSIONS | 34 |
| Appendix A | Calibration and Reduction of Solar Transmissometer Data | 45 |
| A.1 | Solar Power Input to the Transmissometer | 45 |
| A.2 | Calibration Equation | 46 |
| A.3 | Calibration Constant | 47 |
| A.3.1 | Solar Parameters | 47 |
| A.3.2 | Telescope | 47 |
| A.3.3 | Calibration Lamp | 48 |
| A.4 | Measurement Errors of the Signal and Calibration Currents | 50 |
| A.4.1 | Detector Gain | 50 |
| A.4.2 | Dark Current | 50 |

| | | |
|------------|--|----|
| A.4.3 | Reentrant Spectrum | 51 |
| A.5 | Discussion of Previous EK/EG&G Calibrations | 51 |
| A.6 | Differences in Data Reduction for SABLE 89 | 52 |
| Appendix B | File Formats and Computer Programs Used in This Analysis | 54 |
| B.1 | File Format of the Solar Transmissometer Data | 54 |
| B.2 | Computer Programs for Data Analysis | 54 |
| B.2.1 | Program <i>SIGNAL.FOR</i> | 55 |
| B.2.2 | Program <i>RECAL.FOR</i> | 55 |
| B.2.3 | Program <i>REMOVE.FOR</i> | 55 |
| B.2.4 | Program <i>CIRRUS.FOR</i> | 56 |
| B.2.5 | Program <i>STRATO.FOR</i> | 56 |
| B.2.6 | Program <i>TGAPS.FOR</i> | 56 |

Figures

| | | |
|----|--|----|
| 1 | Scatter Plot of $\ln i_{\lambda_s}$ as a Function of $\sec \phi$ for 25 July 1989 | 6 |
| 2 | Scatter Plot of $\ln i_{\lambda_s}$ as a Function of $\sec \phi$ for 28 June 1989 | 6 |
| 3 | Scatter Plot of $\ln i_{\lambda_s}$ as a Function of $\sec \phi$ for 1 July 1989 | 7 |
| 4 | Scatter Plot of $\ln i_{\lambda_s}$ as a Function of $\sec \phi$ for 2 July 1989 | 7 |
| 5 | Scatter Plot of $\ln i_{\lambda_s}$ as a Function of $\sec \phi$ for 6 July 1989 | 8 |
| 6 | Scatter Plot of $\ln i_{\lambda_s}$ as a Function of $\sec \phi$ for 7 July 1989 | 8 |
| 7 | Comparison of Solar Transmissions From the Filament Lamp Calibration Against Those From the Langley Calibration for 25 June 1989 | 9 |
| 8 | Comparison of Solar Transmissions From the Filament Lamp Calibration Against Those From the Langley Calibration for 28 June 1989 | 10 |
| 9 | Comparison of Solar Transmissions From the Filament Lamp Calibration Against Those From the Langley Calibration for 1 July 1989 | 11 |
| 10 | Comparison of Solar Transmissions From the Filament Lamp Calibration Against Those From the Langley Calibration for 2 July 1989 | 12 |
| 11 | Comparison of Solar Transmissions From the Filament Lamp Calibration Against Those From the Langley Calibration for 6 July 1989 | 13 |
| 12 | Comparison of Solar Transmissions From the Filament Lamp Calibration Against Those From the Langley Calibration for 7 July 1989 | 14 |
| 13 | Example of Reduced Solar Transmissions at 532 nm for 6 July 1989 | 15 |
| 14 | Comparisons Between Observed Surface Visibilities at Ascension Island and Visibilities Used for Aerosol Removal as a Function of Time for 25 June 1989 | 17 |
| 15 | Comparisons Between Observed Surface Visibilities at Ascension Island and Visibilities Used for Aerosol Removal as a Function of Time for 28 June 1989 | 17 |

| | | |
|-----|---|----|
| 16 | Comparisons Between Observed Surface Visibilities at Ascension Island and Visibilities Used for Aerosol Removal as a Function of Time for 1 July 1989 | 18 |
| 17 | Comparisons Between Observed Surface Visibilities at Ascension Island and Visibilities Used for Aerosol Removal as a Function of Time for 2 July 1989 | 18 |
| 18 | Comparisons Between Observed Surface Visibilities at Ascension Island and Visibilities Used for Aerosol Removal as a Function of Time for 6 July 1989 | 19 |
| 19 | Comparisons Between Observed Surface Visibilities at Ascension Island and Visibilities Used for Aerosol Removal as a Function of Time for 7 July 1989 | 19 |
| 20 | Values of Transmission as a Function of Time After Removing Aerosol, Molecular, and Solar Zenith Effects With Appropriate and Improper Surface Visibilities in LOWTRAN7 | 20 |
| 21 | Values of Transmission as a Function of Time for 25 June 1989 After Removing Molecular, Aerosol, and Solar Zenith Effects | 21 |
| 22 | Values of Transmission as a Function of Time for 28 June 1989 After Removing Molecular, Aerosol, and Solar Zenith Effects | 21 |
| 23 | Values of Transmission as a Function of Time for 1 July 1989 After Removing Molecular, Aerosol, and Solar Zenith Effects | 22 |
| 24 | Values of Transmission as a Function of Time for 2 July 1989 After Removing Molecular, Aerosol, and Solar Zenith Effects | 22 |
| 25 | Values of Transmission as a Function of Time for 6 July 1989 After Removing Molecular, Aerosol, and Solar Zenith Effects | 23 |
| 26 | Values of Transmission as a Function of Time for 7 July 1989 After Removing Molecular, Aerosol, and Solar Zenith Effects | 23 |
| 27 | Calculated Transmission Through Cirrus Clouds in the Solar Direction Versus Solar Zenith Angle for Cloud Thicknesses of 0.5, 1.0, 1.5, 2.0, and 2.5 km | 28 |
| 28 | Calculated Transmission Through Cirrus Clouds in the Solar Direction Versus Local Time for Ascension Island for Cloud Thicknesses of 0.5, 1.0, 1.5, 2.0, and 2.5 km | 28 |
| 29 | Calculated Transmission Through Stratocumulus Clouds in the Solar Direction Versus Solar Zenith Angle for Cloud Thicknesses of 1, 2, 5, 10, 50, and 100 m | 29 |
| 30 | Calculated Transmission Through Stratocumulus Clouds in the Solar Direction Versus Local Time for Ascension Island for Cloud Thicknesses of 1, 2, 5, 10, 50, and 100 m | 29 |
| 31 | Daily Percent Distributions of Individual Transmission Measurements In Which Only Presumed Occurrences of Cloud Edges and Thin Spots Have Been Included | 31 |
| 32 | Frequency of Occurrence of Cloud Edges and Thin Spots Events Versus Duration Time | 42 |
| A-1 | Spectral Radiance of the Ribbon Filament Lamp, B_c , as a Function of Wavelength | 49 |
| A-2 | Spectral Reflectance of the Parabolic Mirror, R_p as a Function of Wavelength | 49 |
| A-3 | Calibration Ratio, $K(\lambda)$, for the Solar Transmissometer as a Function of Wavelength | 50 |

| | | |
|-----|---|----|
| A-4 | Daily Calibrations of the Solar Transmissometer as Scaled from the Average for SABLE 89 as a Function of Wavelength | 53 |
| B-1 | Example of a File Containing Solar Transmission Data | 54 |

Tables

| | | |
|----|---|----|
| 1 | Dates and Times When the EK/EG&G Solar Transmissometer Was Used During SABLE 89 | 1 |
| 2 | Daily Calibration Factors for the Solar Transmissometer Obtained with the Langley Method | 5 |
| 3 | Surface Visibilities Used in LOWTRAN7 to Remove Aerosol, Molecular, and Zenith Angle Effects From the Solar Transmission Data Taken During SABLE 89 | 16 |
| 4 | Daily Occurrences of Inferred τ_{cld} as a Function of Transmission | 24 |
| 5 | Values of Parameters Used to Estimate the Effects of Forward Scattering on the Transmission Measurements at Ascension Island | 25 |
| 6 | Estimated Cirrus Transmissions on 25 June 1989 | 26 |
| 7 | Daily Percent Distributions of Individual Transmission Measurements In Which Only Presumed Occurrences of Cloud Edges and Thin Spots Have Been Included | 30 |
| 8 | Daily Averages and Standard Deviations of Transmission In Which Only Presumed Occurrences of Cloud Thin Spots and Edges Have Been Included | 31 |
| 9 | Daily Values of $N_{edge}/(N_{edge} + N_{cld})$ for Over Ascension Island | 32 |
| 10 | Times and Durations of Presumed Cloud Edges and Thin Spots for 28 June 1989 at Ascension Island | 34 |
| 11 | Times and Durations of Presumed Cloud Edges and Thin Spots for 1 July 1989 at Ascension Island | 35 |
| 12 | Times and Durations of Presumed Cloud Edges and Thin Spots for 2 July 1989 at Ascension Island | 36 |
| 13 | Times and Durations of Presumed Cloud Edges and Thin Spots for 6 July 1989 at Ascension Island | 38 |

| | | |
|----|---|----|
| 14 | Times and Durations of Presumed Cloud Edges and Thin Spots for 7 July 1989 at Ascension Island | 40 |
| 15 | Frequency of Occurrence of Cloud Edges and Thin Spots Events of Different Time Durations | 41 |

ACKNOWLEDGEMENT

Sparta, Inc. wishes to recognize LTC G.G. Koenig of the Electro-Optics Measurements Branch of the Geophysics Directorate of Phillips Laboratory, who has made extensive contributions to this report. His initial suggestions and comments have formed the framework for this report. Furthermore, since he was on Ascension Island during the SABLE 89 field test, LTC G.G. Koenig has provided an "on-site" knowledge of how the solar transmissometer made its measurements, as well as additional insight into the weather conditions observed on the island.

ANALYSIS OF SOLAR TRANSMISSION DATA FROM SABLE 89

1 INTRODUCTION

The Geophysics Directorate of Phillips Laboratory (PL/GP), in collaboration with the Royal Signal and Radar Establishment (RSRE), has performed an extensive series of aerosol laser backscatter measurements at Ascension Island as part of the South Atlantic Backscatter Lidar Experiment (SABLE)¹. A series of experiments took place in the fall of 1988 (SABLE 88) and a second in the summer of 1989 (SABLE 89) as a part of a continuing effort to study the aerosol backscatter characteristics of the atmosphere. Catalogs of information and available data from SABLE 88 and SABLE 89 have been assembled^{2,3}.

During SABLE 89, an EK/EG&G solar transmissometer was operated on Ascension Island. Details about the instrumentation are given elsewhere³. As the transmissometer tracked the sun, the system was operated alternately in one of the following modes: at 532 nm as a function of time, and scans of solar spectrum from 400 to 1200 nm. (Note that due to instrument problems, the useable spectral region was from 450 to 1000 nm.) For reference, Table 1 gives the dates and times when the solar transmissometer was operated. Clearly, the series of measurements form an extensive data base with which one can explore the properties of aerosols and clouds over Ascension Island.

¹ Alejandro, S.B., Koenig, G.G., Vaughn, J.M., and Davies, P.H. (1990) "SABLE: A South Atlantic Aerosol Backscatter Measurement Program," *Bul. Am. Meteor. Soc.*, 71:281-287.

² Hummel, J.R., and Longtin, D.R. (1992) "Catalog of Data and Information from the 1988 SABLE Mission," in progress.

³ Hummel, J.R., and Longtin, D.R. (1992) "Catalog of Data and Information from the 1989 SABLE Mission," in progress.

Table 1. Dates and Times When the EK/EG&G Solar Transmissometer Was Used During SABLE 89. All listed times are local time which is the same as GMT for Ascension Island

| DATE | 532 nm SCAN TIMES | SOLAR SCAN TIMES |
|--------------|----------------------------|----------------------------|
| 25 June 1989 | 11:43-12:01 | 12:04-12:16 |
| | 12:19-12:36 | 12:38-12:50 |
| | 12:54-13:11 | 13:14-13:26 |
| | 13:29-13:46 | 13:49-14:01 |
| | 14:05-14:22 | 14:27-14:31 (partial scan) |
| 28 June 1989 | 13:31-14:14 | 14:16-14:23 |
| | 14:27-15:09 | 15:12-15:24 |
| | 15:27-15:55 | |
| | 16:23-17:06 | 17:09-17:22 |
| | 17:24-17:38 | |
| 1 July 1989 | 11:41-12:54 | 12:57-13:13 |
| | 13:16-14:03 | 14:05-14:18 |
| | 14:22-15:07 | 15:09-15:24 |
| | 15:31-16:13 | |
| 2 July 1989 | 10:21-11:07 | 11:18-11:35 |
| | 11:39-12:29 | 12:31-12:45 |
| | 12:48-13:35 | 13:37-13:51 |
| | 13:54-14:44 | 14:47-15:01 |
| | 15:04-15:56 | 15:59-16:14 |
| | 17:21-18:01 | |
| 6 July 1989 | 09:33-10:18 | 10:21-10:32 |
| | 10:39-11:25 | 11:28-11:40 |
| | 11:43-12:27 | 12:30-12:43 |
| | 12:52-13:44 | 13:47-13:51 (partial scan) |
| | 14:03-14:53 | 14:56-15:09 |
| | 15:12-15:58 | 16:01-16:14 |
| | 16:17-17:01 | 17:03-17:15 |
| | 17:18-18:02 | 18:04-18:19 |
| | 18:23-18:37 (poor quality) | |
| 7 July 1989 | 10:31-11:19 | 11:22-11:35 |
| | 11:38-12:23 | 12:25-12:39 |
| | 12:43-13:28 | 13:30-13:42 |
| | 13:46-14:29 | 14:32-14:50 |
| | 14:53-15:42 | 15:47-16:01 |
| | 16:07-17:06 | 17:10-17:22 |
| | 17:26-18:12 | 18:15-18:28 |
| | 18:30-18:54 | |

1.1 Purpose and Organization of Report

The purpose of this report is to analyze measurements from the EK/EG&G solar transmissometer. The focus of this report will be the transmission data at 532 nm versus time partly because the solar scans suffered from instrumentation problems. Chapter 2 validates the calibration procedure for the transmission data using the Langley method. Chapter 3 investigates the properties of aerosols and clouds at Ascension Island using the data base of solar transmissometer measurements. Specifically, solar transmissions at 532 nm will be used to study the properties of cirrus and stratocumulus clouds near Ascension Island. Finally, Chapter 4 presents a summary of the results in this report. For reference, Appendix A describes the standard procedure for calibrating the solar transmissometer. Finally, Appendix B gives brief descriptions of computer programs that were developed to analyze the solar transmissometer data, as well as details about how the transmission data files are formatted.

2 VALIDATION OF SOLAR TRANSMISSION MEASUREMENTS

2.1 Concerns About Instrument Calibration

As the solar transmissometer tracked the sun, it measured an electrical current (in nanoamperes) which was then converted to a solar transmission using calibration factors that were based on the current from a filament lamp of known spectral intensity. Unfortunately, the system was very old and there was some question about the quality of the filament lamp. Additionally, the integrating sphere was damaged and there was a re-entrant spectrum problem. An attempt was made to compensate for these problems during SABLE 89, however it is recognized that these corrections are no more than stopgap measures.

2.2 Recalibration Using the Langley Method

As an independent check, the solar transmission at 532 nm has been derived directly from the measured solar signal using the Langley calibration method. The Langley method is an application of Beer's law which can be expressed as

$$\tau_{\lambda} = \exp \left[- \int_0^L k_{\lambda}(l) dl \right] \quad (1)$$

where τ_{λ} is the monochromatic transmittance, $k_{\lambda}(l)$ is the extinction coefficient including molecular and aerosol effects, and $dl = \sec \phi dz$. Clearly, Eq. 1 assumes that atmospheric emission is small, which is reasonable at solar wavelengths, and multiple scattering is insignificant. In the Langley method, the calibration factor is defined as $K_{\lambda} \equiv \tau_{\lambda}/i_{\lambda_s}$ where i_{λ_s} is the measured solar signal at the wavelength of interest. Thus, Eq. 1 can be rewritten as

$$\ln i_{\lambda_s} = - \ln K_{\lambda} - \sec \phi \int_0^{\infty} k_{\lambda}(z) dz \quad (2)$$

where ϕ is the solar zenith angle and z is altitude. Assuming the integral in Eq. 2 is relatively constant over the course of a day (*i.e.*, a range of $\sec \phi$), the expression is linear in $\ln i_{\lambda_s}$ and $\sec \phi$ to a good approximation. (For Ascension Island, this is especially true given the high degree of horizontal homogeneity in that area.) Due to the earth's curvature, however, the approximation is only good for solar zenith angles less than 70 degrees. The calibration factor then is found by plotting measured values of $\ln i_{\lambda_s}$ versus $\sec \phi$ and extending a "best fit" line back to $\sec \phi = 0$. In the Langley method, note that a calibration factor is extremely sensitive to the best fit line drawn because it is defined as the exponential of the axis intercept.

Scatter plots of $\ln i_{\lambda_s}$ versus $\sec \phi$ were constructed for each day of solar transmission data in SABLE 89. For reference, these plots are shown in Figures 1 through 6. The Figures also show the best fit lines that were drawn for calibration factors. Note that deviant points below the linear envelope are due to clouds blocking the sun, and they are not used in the Langley method. Also when drawing the best fit lines, only data for $\sec \phi$ less than 3.0 (*i.e.*, solar zenith angles less than 70°) were considered, because Eq. 2 breaks down when the sun is low in the sky. Calibration factors could have been obtained with a least squares approach as opposed to a

graphical approach, but a least squares approach would remain somewhat subjective because it would be based on an arbitrary selection of data points that make up the linear envelope. Table 2 lists the daily calibration factors that were derived from Figures 1 through 6.

Figures 7 through 12 compare daily solar transmissions at 532 nm as derived with the filament lamp calibration and Langley calibration. Generally speaking, there is reasonable agreement between the two calibration methods. In Figures 11 and 12, which represent 6 and 7 July 1989, respectively, there is near perfect agreement between the two methods. The extensive data sets on 6 July and 7 July may account for the exceptional agreement because the calibration factors for the Langley method can be obtained with more reliable best fit lines. For 25 and 28 June 1989, the Langley transmissions are about 5% less than the filament lamp transmissions. The largest differences exist on 1 and 2 July where transmissions derived from the Langley method are about 10% less than those from the filament lamp. It is difficult to say which calibration technique is "correct" because both methods have their limitations. However, the transmissions derived from the Langley method appear to show better agreement with the day-to-day trends in observed surface visibility at Ascension Island (see Section 3.1).

Table 2. Daily Calibration Factors for the Solar Transmissometer Obtained with the Langley Method

| DATE | $\ln K_\lambda$ | K_λ |
|--------------|-----------------|-------------|
| 25 June 1989 | 4.3916 | 80.775 |
| 28 June 1989 | 4.3533 | 77.737 |
| 1 July 1989 | 4.3800 | 79.838 |
| 2 July 1989 | 4.3950 | 81.045 |
| 6 July 1989 | 4.3633 | 78.518 |
| 7 July 1989 | 4.4166 | 82.819 |

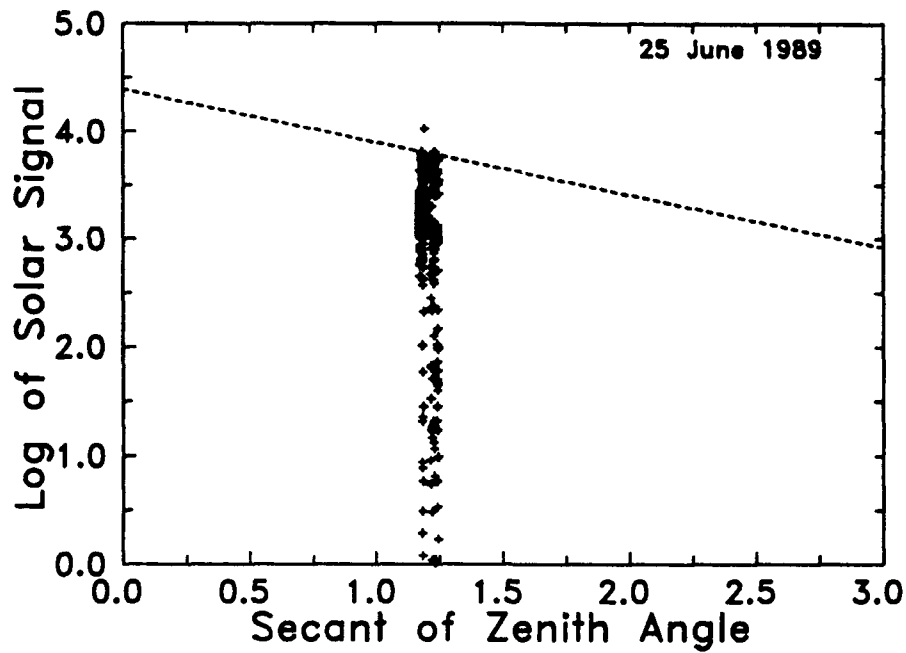


Figure 1. Scatter Plot of $\ln i_{\lambda_s}$ as a Function of $\sec \phi$ for 25 July 1989. The dashed line is the best fit line for the Langley method. Because they represent transmissions through clouds, values of $\ln i_{\lambda_s}$ less than 0.0 are not plotted to reduce clutter

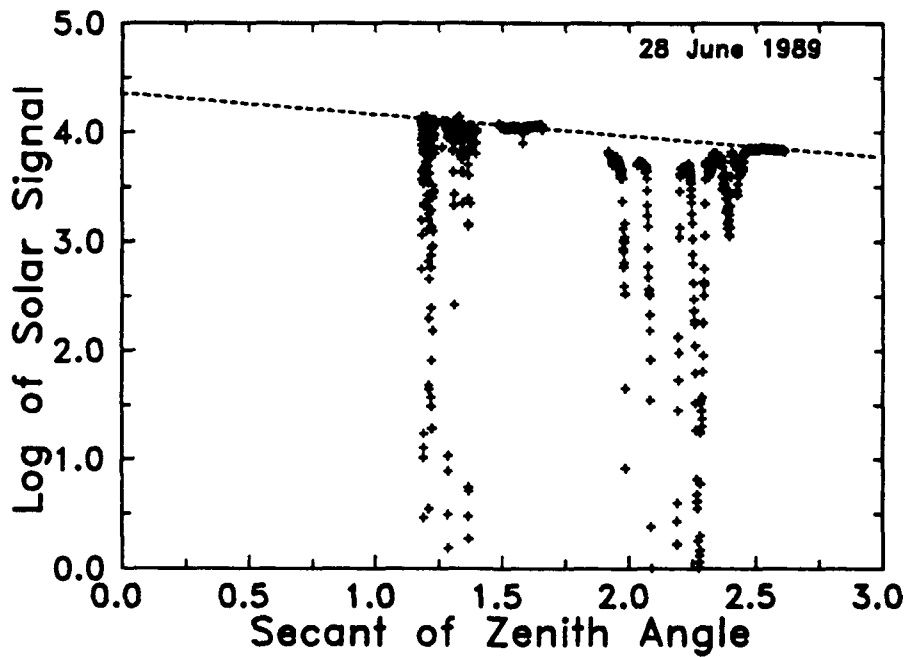


Figure 2. Scatter Plot of $\ln i_{\lambda_s}$ as a Function of $\sec \phi$ for 28 June 1989. The dashed line is the best fit line for the Langley method. Because they represent transmissions through clouds, values of $\ln i_{\lambda_s}$ less than 0.0 are not plotted to reduce clutter

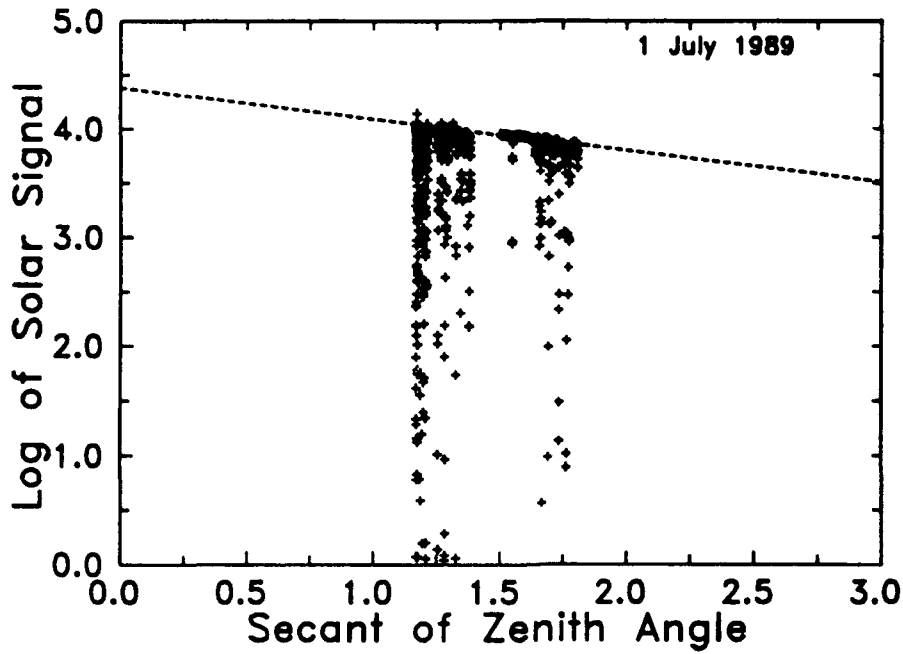


Figure 3. Scatter Plot of $\ln i_{\lambda_s}$ as a Function of $\sec \phi$ for 1 July 1989. The dashed line is the best fit line for the Langley method. Because they represent transmissions through clouds, values of $\ln i_{\lambda_s}$ less than 0.0 are not plotted to reduce clutter

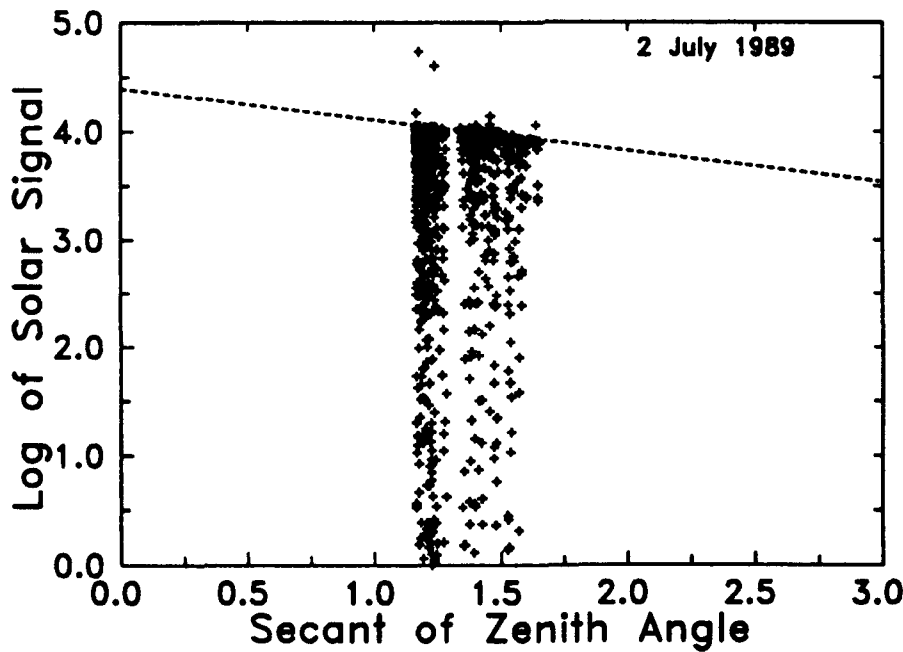


Figure 4. Scatter Plot of $\ln i_{\lambda_s}$ as a Function of $\sec \phi$ for 2 July 1989. The dashed line is the best fit line for the Langley method. Because they represent transmissions through clouds, values of $\ln i_{\lambda_s}$ less than 0.0 are not plotted to reduce clutter

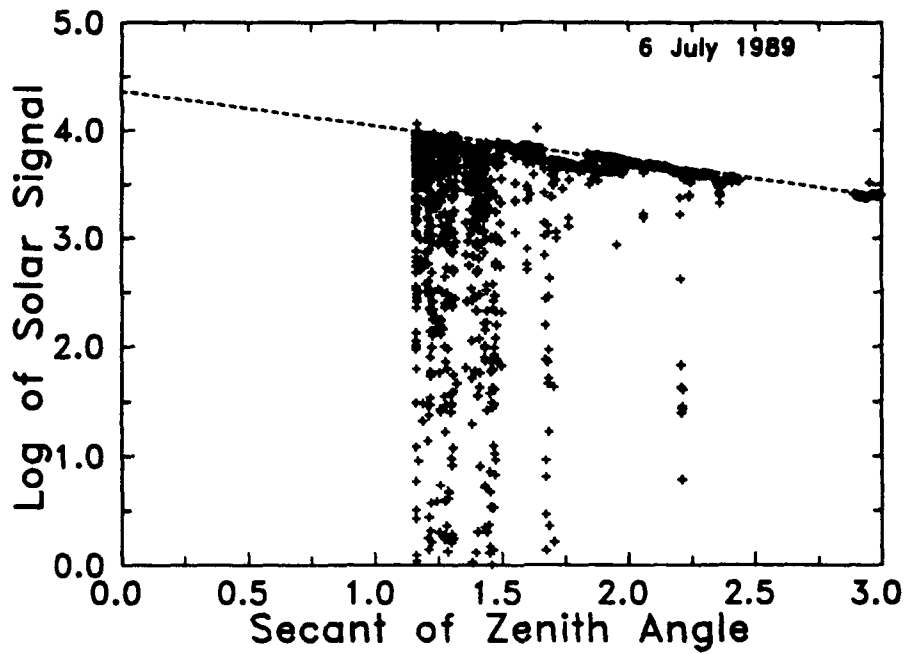


Figure 5. Scatter Plot of $\ln i_{\lambda_s}$ as a Function of $\sec \phi$ for 6 July 1989. The dashed line is the best fit line for the Langley method. Because they represent transmissions through clouds, values of $\ln i_{\lambda_s}$ less than 0.0 are not plotted to reduce clutter

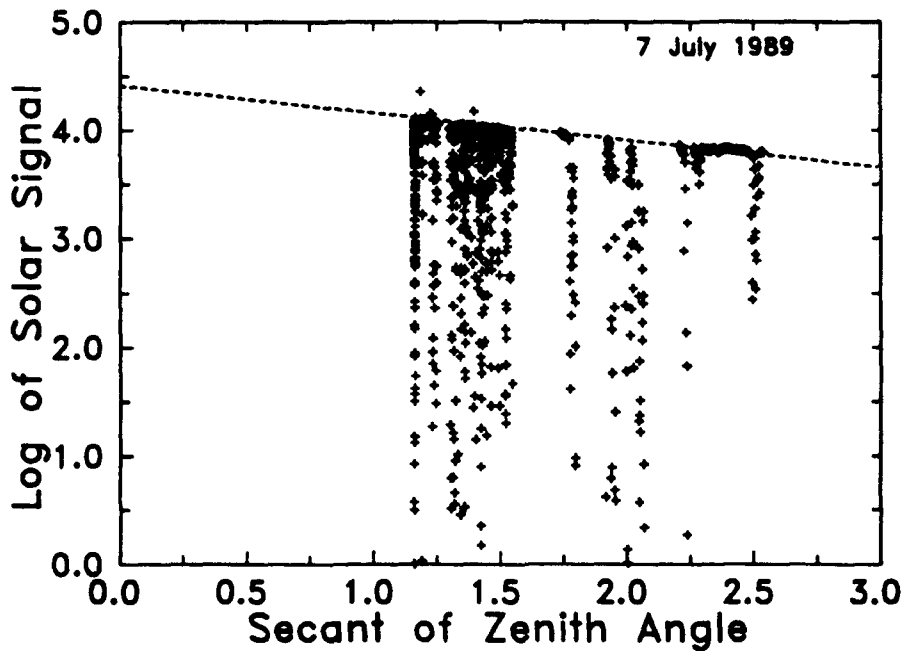


Figure 6. Scatter Plot of $\ln i_{\lambda_s}$ as a Function of $\sec \phi$ for 7 July 1989. The dashed line is the best fit line for the Langley method. Because they represent transmissions through clouds, values of $\ln i_{\lambda_s}$ less than 0.0 are not plotted to reduce clutter

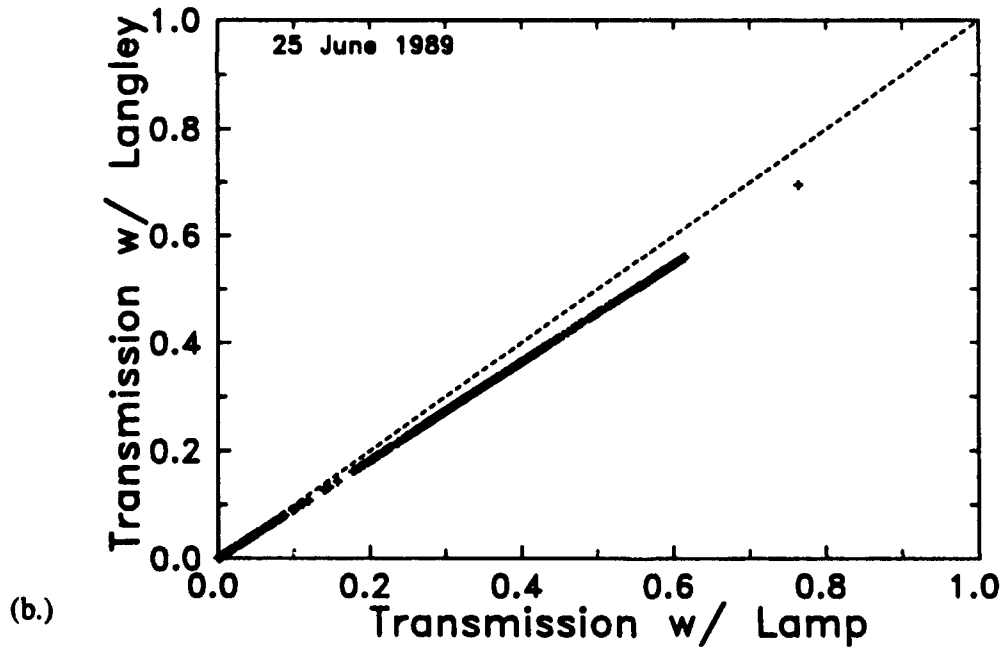
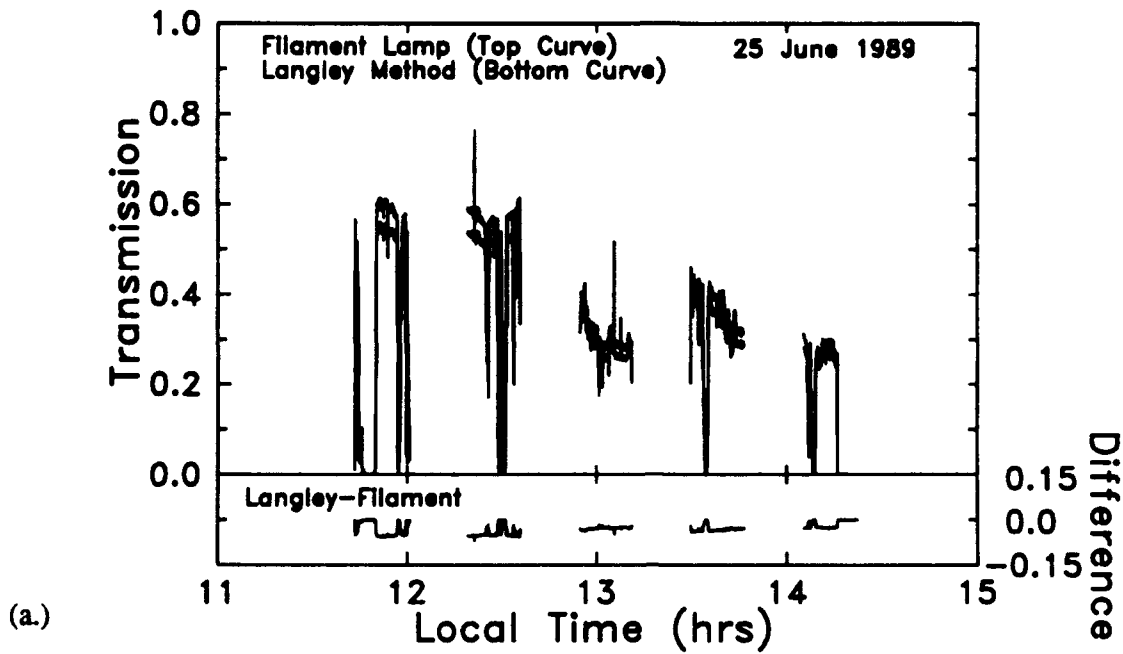


Figure 7. Comparison of Solar Transmissions From the Filament Lamp Calibration Against Those From the Langley Calibration for 25 June 1989. In (a.), transmissions from each calibration and their differences are shown as a function of time. In (b.), corresponding transmission measurements from each calibration are shown in terms of a scatter plot

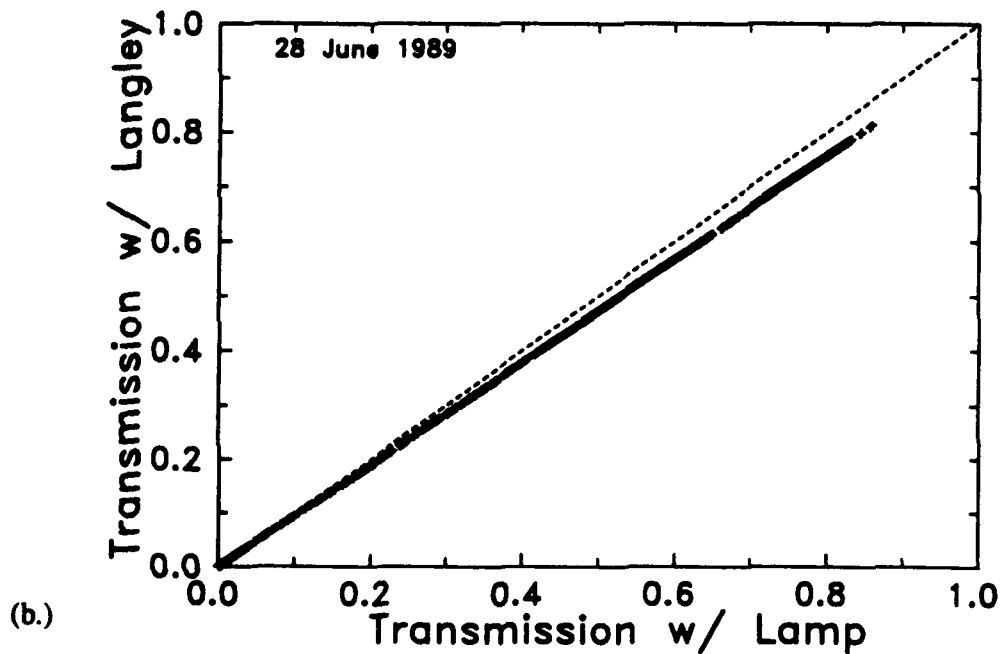
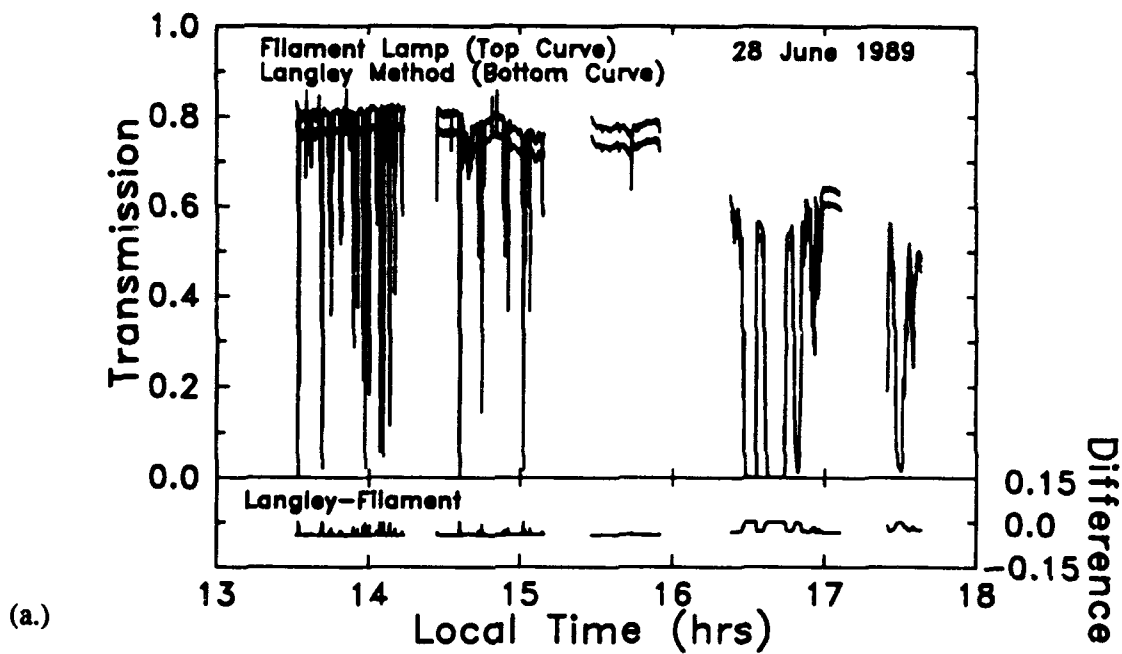


Figure 8. Comparison of Solar Transmissions From the Filament Lamp Calibration Against Those From the Langley Calibration for 28 June 1989. In (a.), transmissions from each calibration and their differences are shown as a function of time. In (b.), corresponding transmission measurements from each calibration are shown in terms of a scatter plot

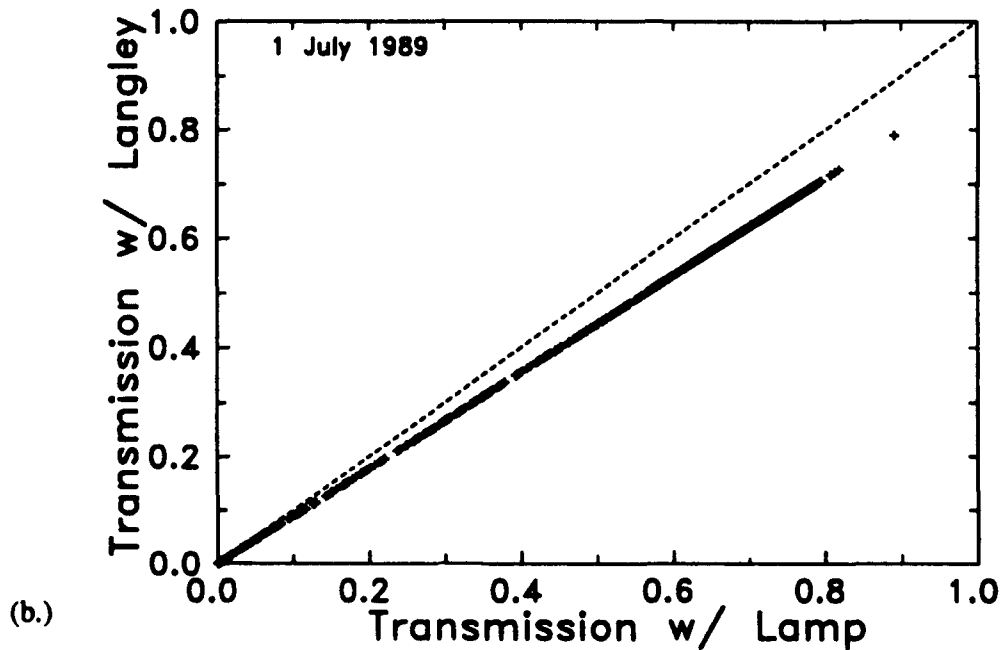
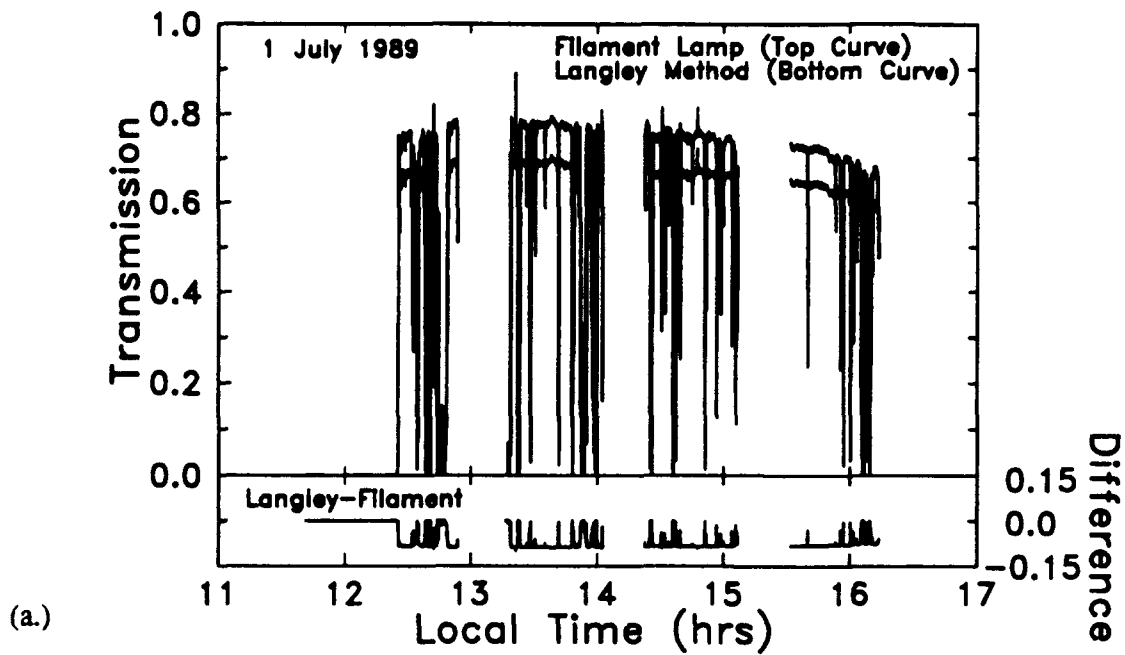


Figure 9. Comparison of Solar Transmissions From the Filament Lamp Calibration Against Those From the Langley Calibration for 1 July 1989. In (a.), transmissions from each calibration and their differences are shown as a function of time. In (b.), corresponding transmission measurements from each calibration are shown in terms of a scatter plot

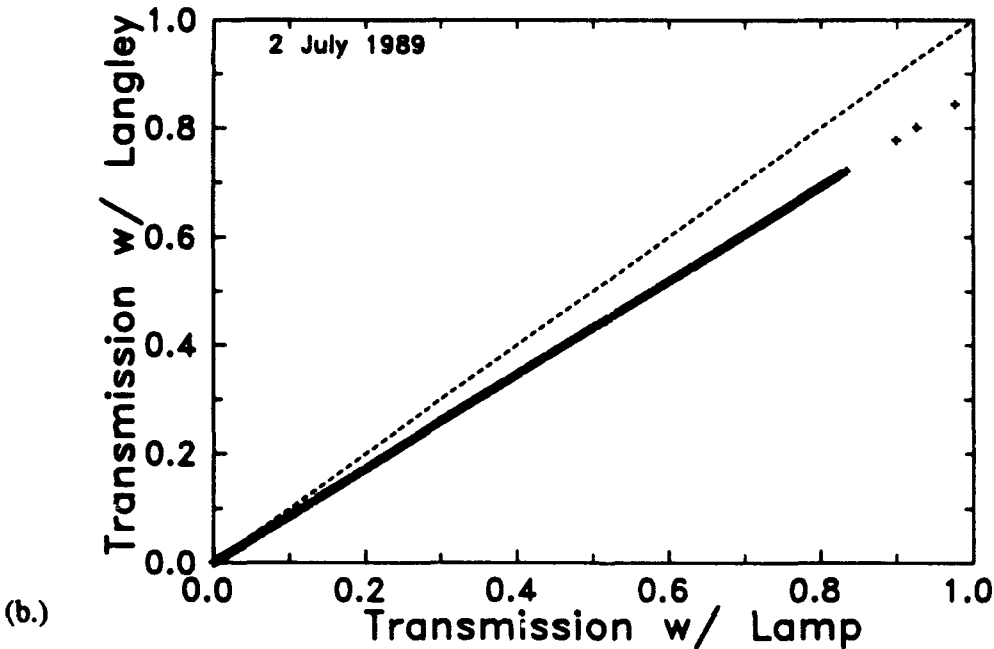
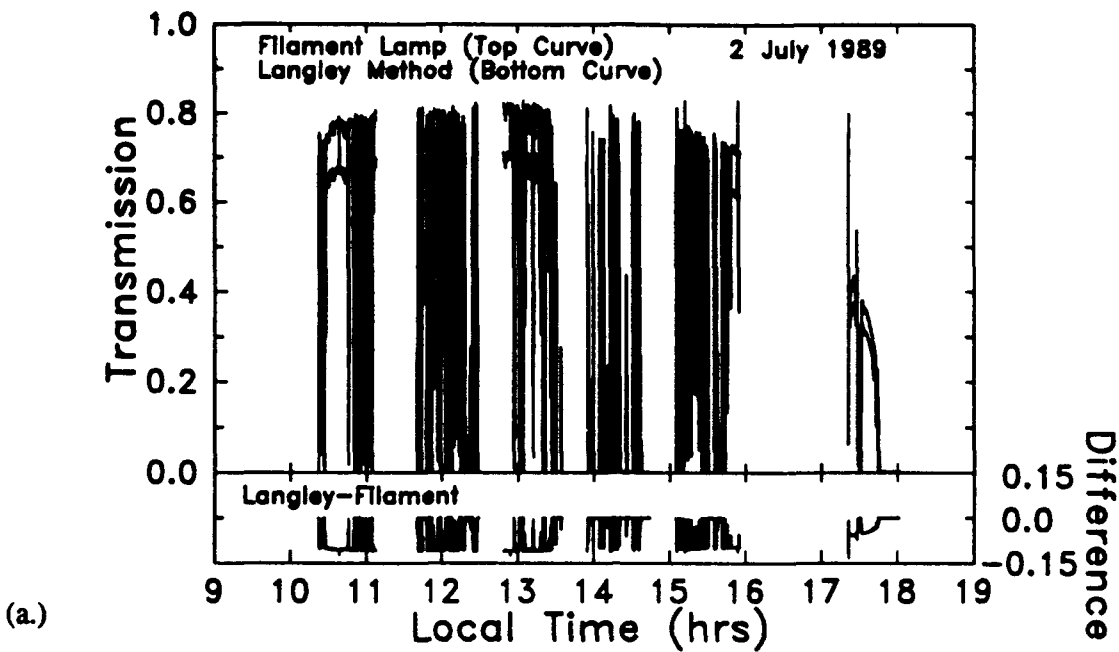


Figure 10. Comparison of Solar Transmissions From the Filament Lamp Calibration Against Those From the Langley Calibration for 2 July 1989. In (a.), transmissions from each calibration and their differences are shown as a function of time. In (b.), corresponding transmission measurements from each calibration are shown in terms of a scatter plot

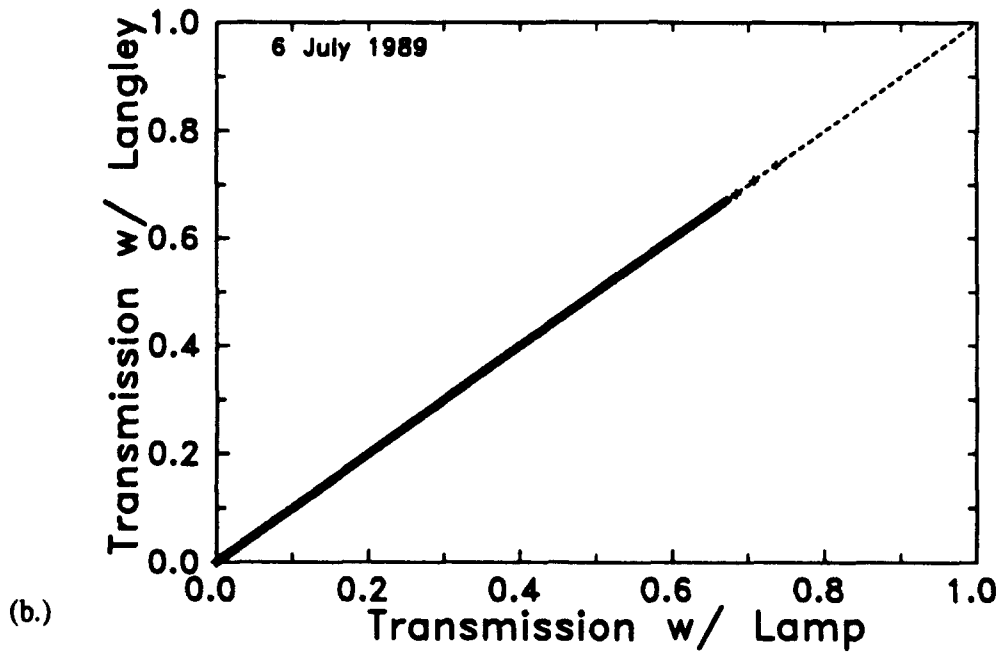
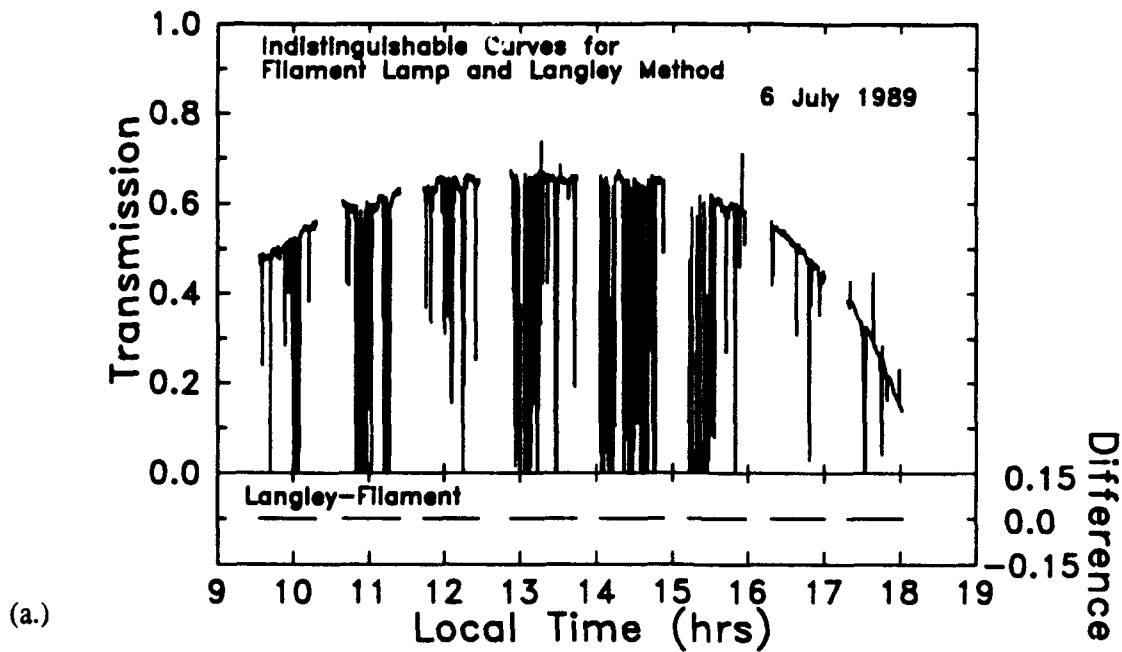


Figure 11. Comparison of Solar Transmissions From the Filament Lamp Calibration Against Those From the Langley Calibration for 6 July 1989. In (a.), transmissions from each calibration and their differences are shown as a function of time. In (b.), corresponding transmission measurements from each calibration are shown in terms of a scatter plot

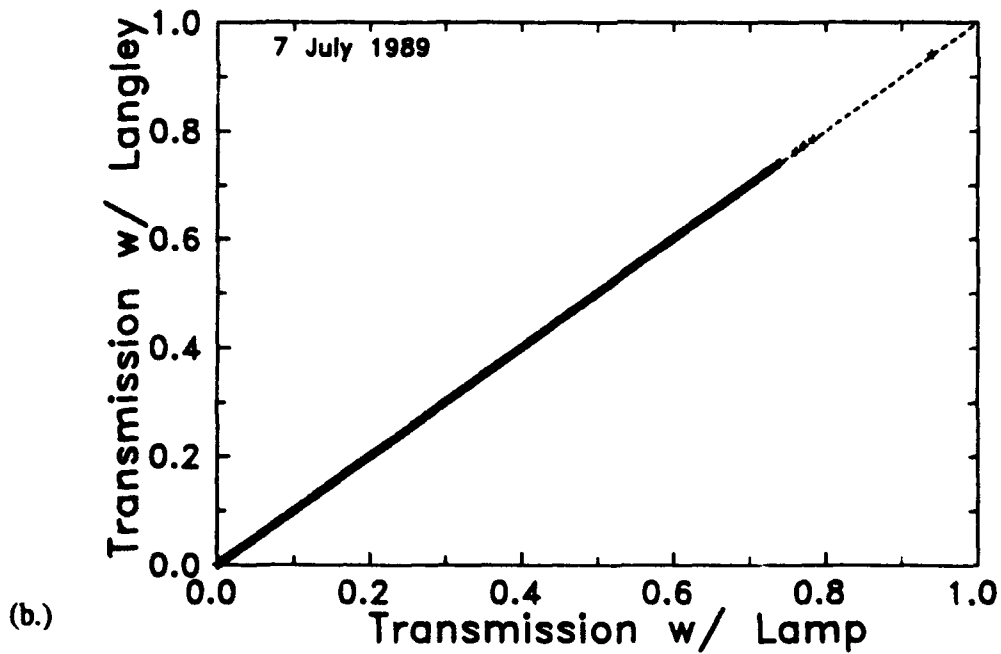
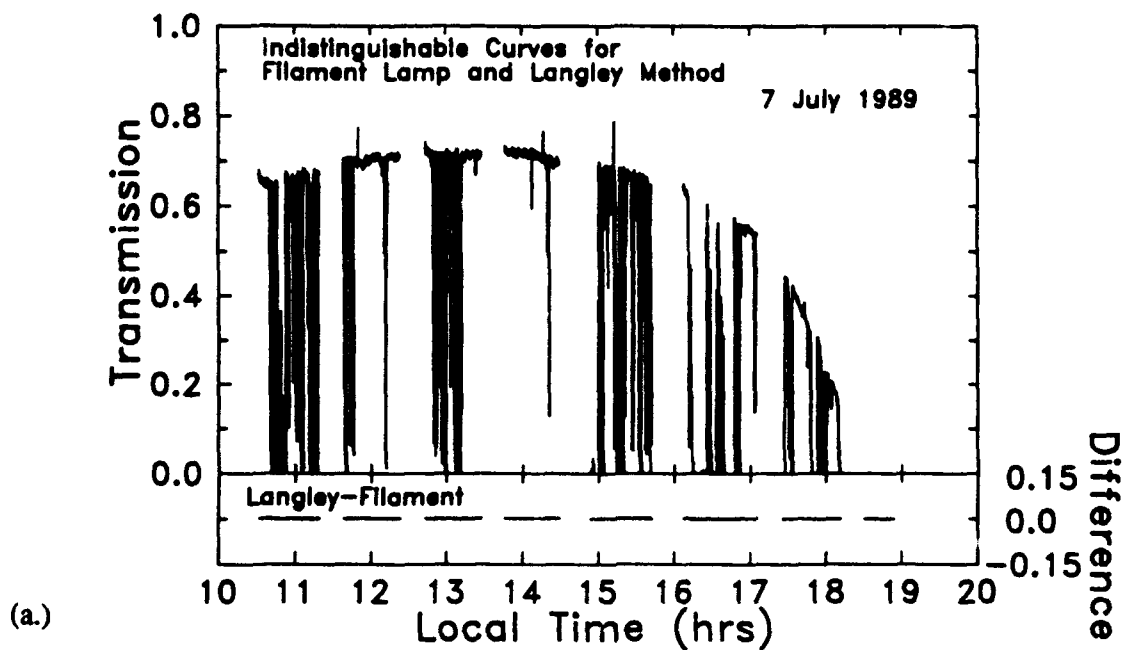


Figure 12. Comparison of Solar Transmissions From the Filament Lamp Calibration Against Those From the Langley Calibration for 7 July 1989. In (a.), transmissions from each calibration and their differences are shown as a function of time. In (b.), corresponding transmission measurements from each calibration are shown in terms of a scatter plot

3 ANALYSIS OF SOLAR TRANSMISSOMETER DATA AT 532 nm

Close examination of solar transmissometer data at 532 nm indicates times when transmissions are greatly reduced, but not zero. An example of this behavior is shown in Figure 13. The reduced transmissions are likely due to the blockage of the sun by boundary layer stratocumulus or cirrus clouds. In the case of boundary layer stratocumulus, reduced transmissions are possible when the cloud is thin or near the cloud edges. Since most radiative and climate models assume cumuloform clouds to be optically thick (*i.e.*, no solar transmission), additional information about cloud transmission properties can be obtained from the solar transmission data from SABLE 89.

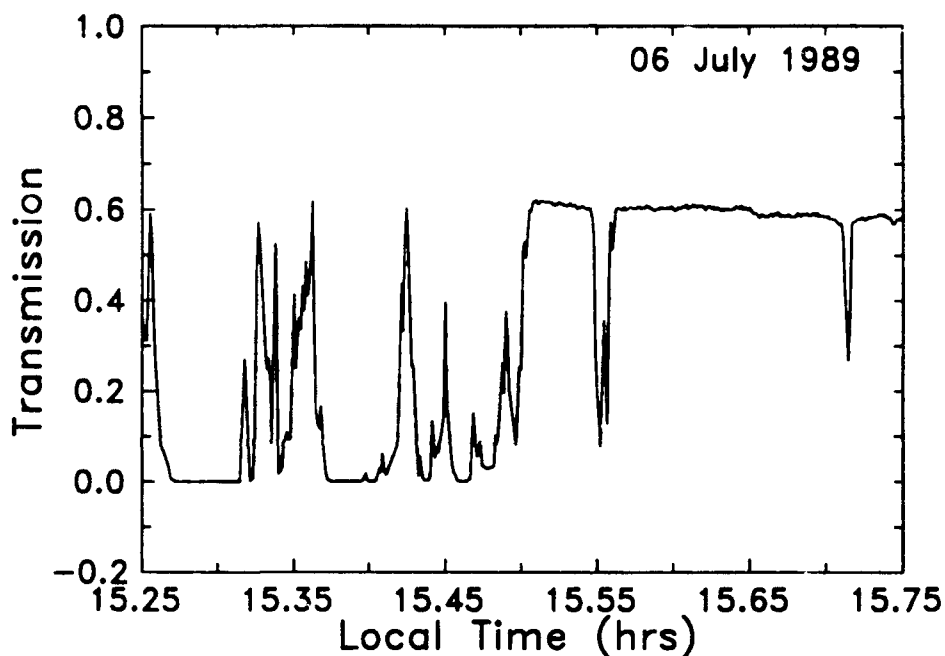


Figure 13. Example of Reduced Solar Transmissions at 532 nm for 6 July 1989.

3.1 Removal Of Aerosol Effects

In order to study the transmission properties of clouds over time, it is first necessary to separate and remove the aerosol and molecular transmissions from the measured solar transmissions to get the cloud transmissions. To do this, the measured solar transmission, τ_{mea} , was expressed as

$$\tau_{mea} = \tau_{clr}\tau_{cld} \quad (3)$$

where τ_{clr} is the atmospheric transmission including aerosol, molecular and zenith angle effects, and τ_{cld} is the transmission due to clouds. Values of τ_{clr} were computed using LOWTRAN7⁴.

⁴ Kneizys, F.X., Shettle, E.P., Abreu, L.W., Chetwynd, J.H., Anderson, G.P., Gallery, W.O.,

The procedure was to calculate τ_{clr} as a function of solar zenith angle assuming steady state aerosol loading in the boundary layer. (With LOWTRAN7, boundary layer aerosol loading is defined by the surface visibility.) Given a knowledge of the solar zenith angle at Ascension Island versus time, the measured transmissions were then divided by zenith angle dependent values of τ_{clr} for an appropriate surface visibility such that the resulting envelope of transmissions was as close to 1.0 as possible. When generating values of τ_{clr} with LOWTRAN7, the default boundary layer height of 2 km was used because it consistently agreed with lidar backscatter and rawinsonde measurements near Ascension Island during SABLE 89.

For each day of transmission data, aerosol effects were removed using iterative guesses on surface visibility until the best results were achieved. Table 3 lists the final surface visibilities that were adopted in LOWTRAN7 to remove aerosol effects. For reference, Figures 14 through 19 compare these "inferred" values against observed surface visibilities at Ascension Island. The comparisons show very good agreement for 1, 2, 6, and 7 July 1989, but large discrepancies exist for 25 and 28 June 1989. The discrepancies for 25 June occur partly because the presence of cirrus clouds on that day cause the envelope to be poorly defined which makes aerosol removal somewhat arbitrary. For 28 June 1989, it is unclear why the inferred visibility is much greater than observed values. However, some of the observed surface visibilities on 28 June 1989 are greater than 70 km, and they may only be estimates because island locations usually lack distant reference points to accurately determine the surface visibility in a very clean atmosphere.

Table 3. Surface Visibilities Used in LOWTRAN7 to Remove Aerosol, Molecular, and Zenith Angle Effects From the Solar Transmission Data Taken During SABLE 89

| DATE | LOWTRAN7 |
|--------------|----------------------------|
| | SURFACE VISIBILITY (km) |
| 25 June 1989 | 20 |
| 28 June 1989 | 130 |
| 1 July 1989 | 48 |
| 2 July 1989 | 52 |
| 6 July 1989 | 37 |
| 7 July 1989 | 60 |

Interestingly, the choice of surface visibility in LOWTRAN7 affects the shape of an envelope, besides shifting its absolute value about 1.0. An example of this behavior is shown in Figure 20 which shows initial attempts to remove aerosol and molecular effects for 7 July 1989 using other

Selby, J.E.A., and Clough, S.A. (1988) "Users Guide to LOWTRAN7," Air Force Geophysics Laboratory, Hanscom AFB, MA, AFGL-TR-88-0177, ADA206773.

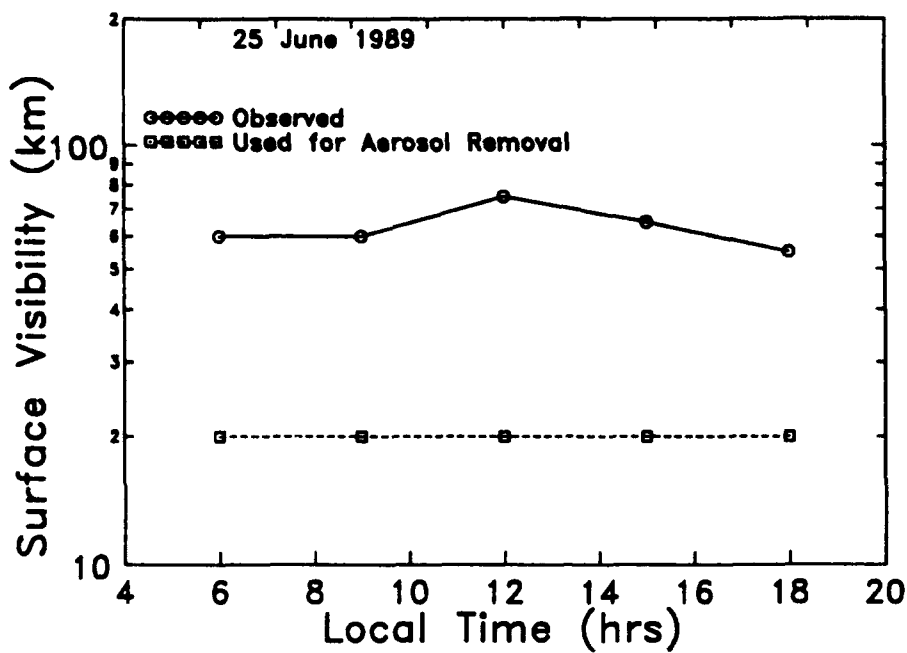


Figure 14. Comparisons Between Observed Surface Visibilities at Ascension Island and Visibilities Used for Aerosol Removal as a Function of Time for 25 June 1989

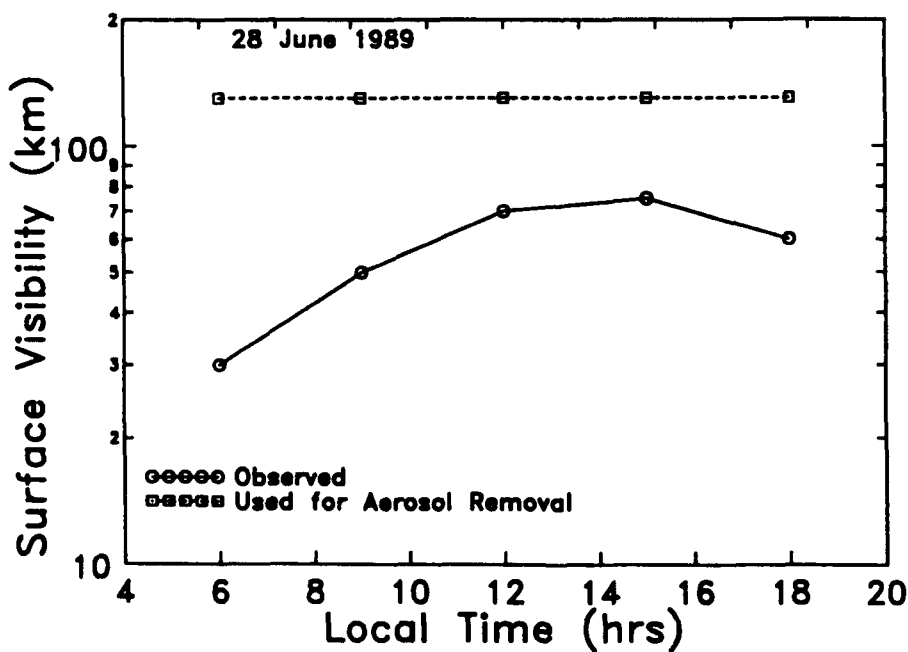


Figure 15. Comparisons Between Observed Surface Visibilities at Ascension Island and Visibilities Used for Aerosol Removal as a Function of Time for 28 June 1989

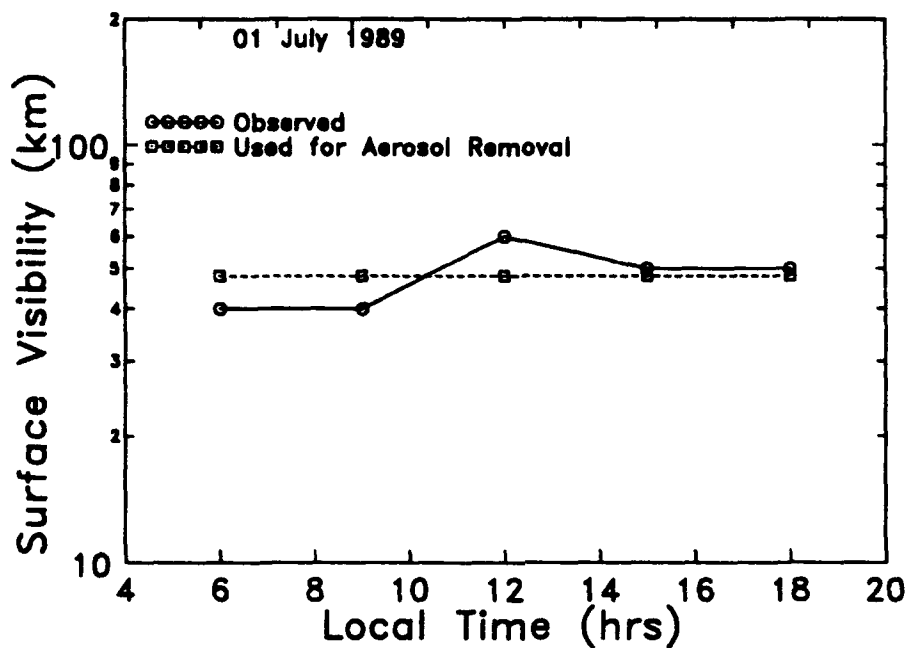


Figure 16. Comparisons Between Observed Surface Visibilities at Ascension Island and Visibilities Used for Aerosol Removal as a Function of Time for 1 July 1989

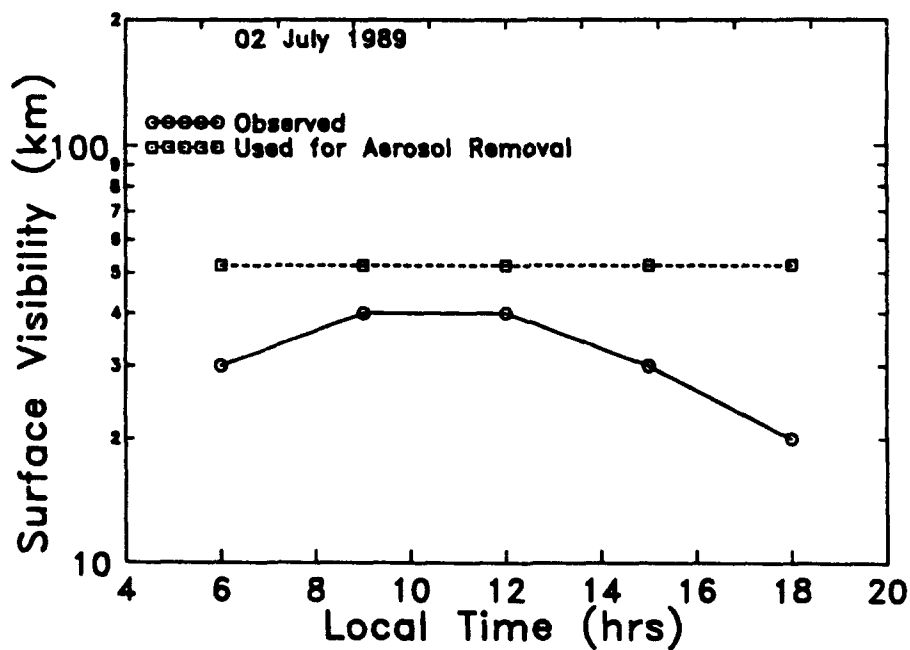


Figure 17. Comparisons Between Observed Surface Visibilities at Ascension Island and Visibilities Used for Aerosol Removal as a Function of Time for 2 July 1989

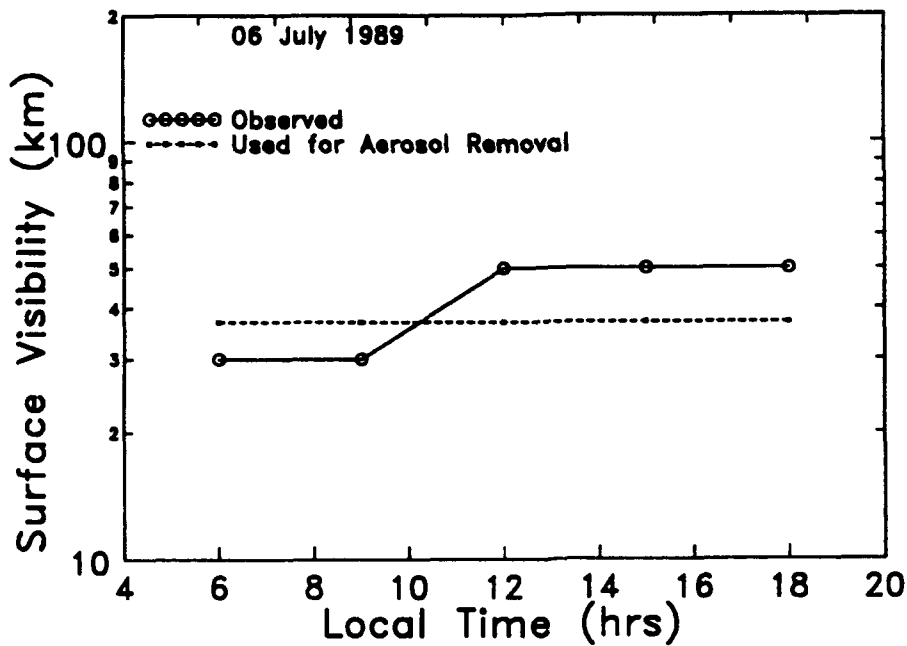


Figure 18. Comparisons Between Observed Surface Visibilities at Ascension Island and Visibilities Used for Aerosol Removal as a Function of Time for 6 July 1989

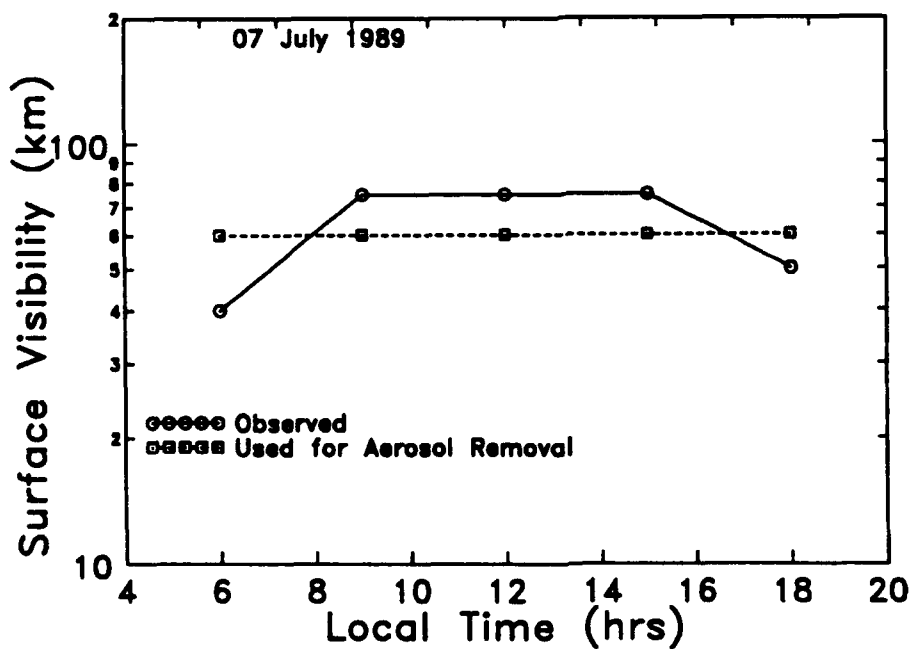


Figure 19. Comparisons Between Observed Surface Visibilities at Ascension Island and Visibilities Used for Aerosol Removal as a Function of Time for 7 July 1989

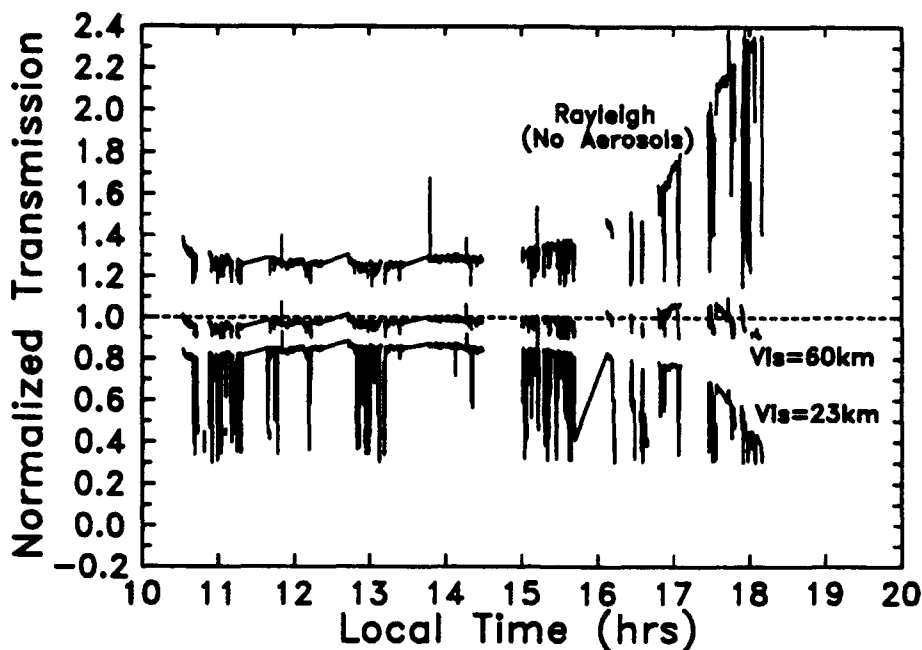


Figure 20. Values of Transmission as a Function of Time After Removing Aerosol, Molecular, and Solar Zenith Effects With Appropriate and Improper Surface Visibilities in LOWTRAN7. For illustrative purposes, only the data depicting the envelopes are shown. Note the distortion of the envelope after 1500 hr when the sun is low in the sky. Measurements for 7 July 1989 were used here

surface visibilities. Clearly, improper surface visibilities cause the envelope to become distorted, especially when the sun is low in the sky.

Figures 21 through 26 show daily transmission values after the aerosol, molecular, and zenith angle effects were removed. Generally, the figures indicate that the technique works well for most days, in that the envelopes are relatively flat and show little diurnal trend. Perhaps the only exception is near sunset (*i.e.*, local times after 1730 hrs) where the envelopes gradually taper below 1.0, as seen on 2 July, 6 July, and 7 July 1989. This behavior may be related to small differences between the actual and modeled values for the height and/or aerosol extinction profile of the boundary layer because their effects on the solar transmissions become more pronounced at low solar zenith angles. Additionally, a time dependent surface visibility may improve the normalization process for a few time periods, although the observed surface visibilities do not suggest too much diurnal variation. On 2 July 1989, for example, the envelope between 1700 and 1800 hrs shows a 10% departure from 1.0 plus a gradually tapering off. This behavior is likely due to "real" changes in the surface visibility as suggested by a marked drop in the observed surface visibility between 1500 and 1800 hrs local time (see Figure 17).

Initially, only a limited series of simple statistics was performed on the data in Figures 21 through 26. For example, Table 4 groups daily values of the inferred τ_{cld} into equally spaced transmission bins. Clearly, values of τ_{cld} greater than 0.9 represent clear skies or extremely thin

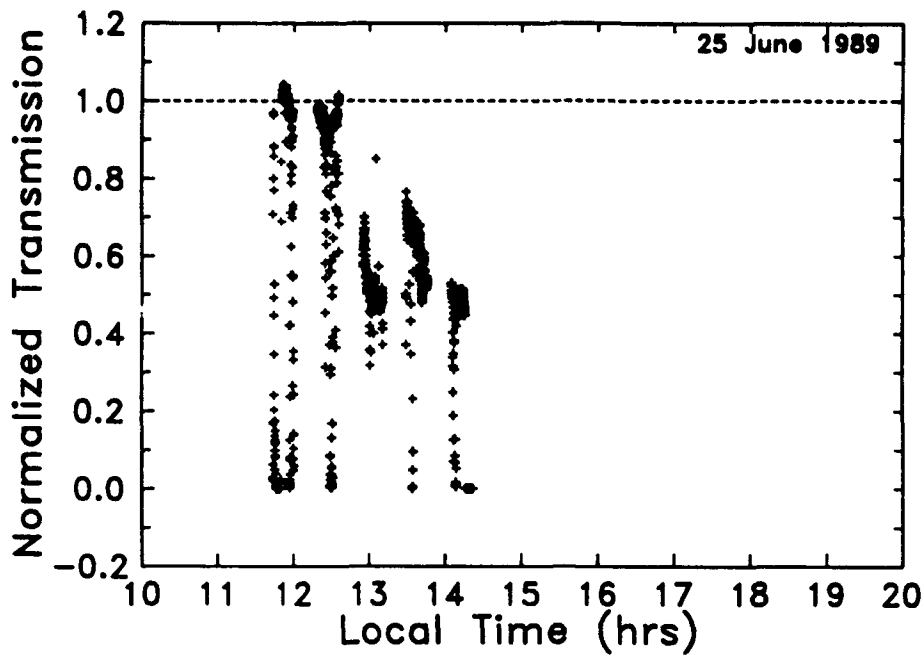


Figure 21. Values of Transmission as a Function of Time for 25 June 1989 After Removing Molecular, Aerosol, and Solar Zenith Effects

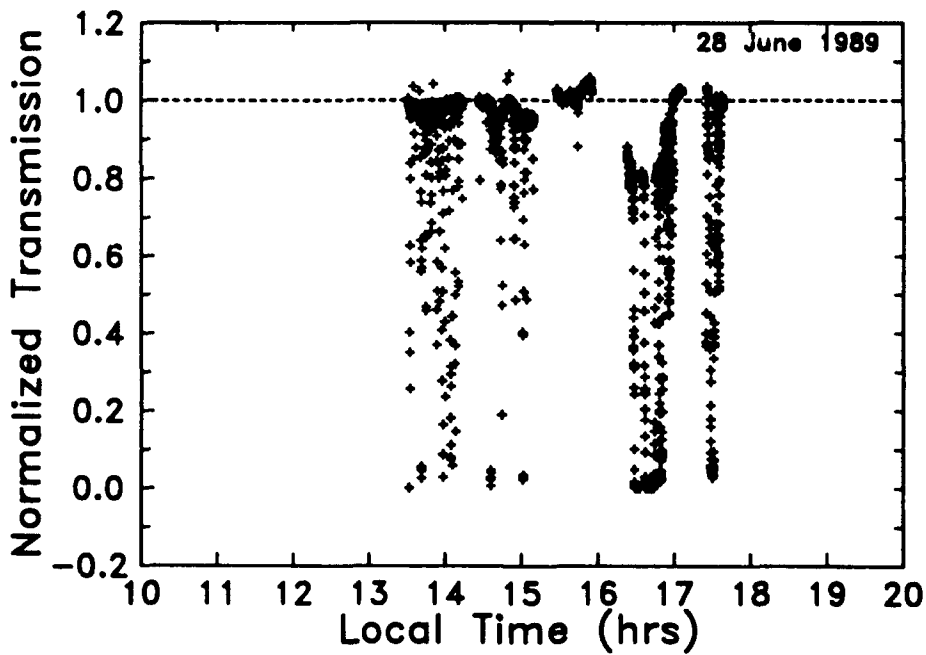


Figure 22. Values of Transmission as a Function of Time for 28 June 1989 After Removing Molecular, Aerosol, and Solar Zenith Effects

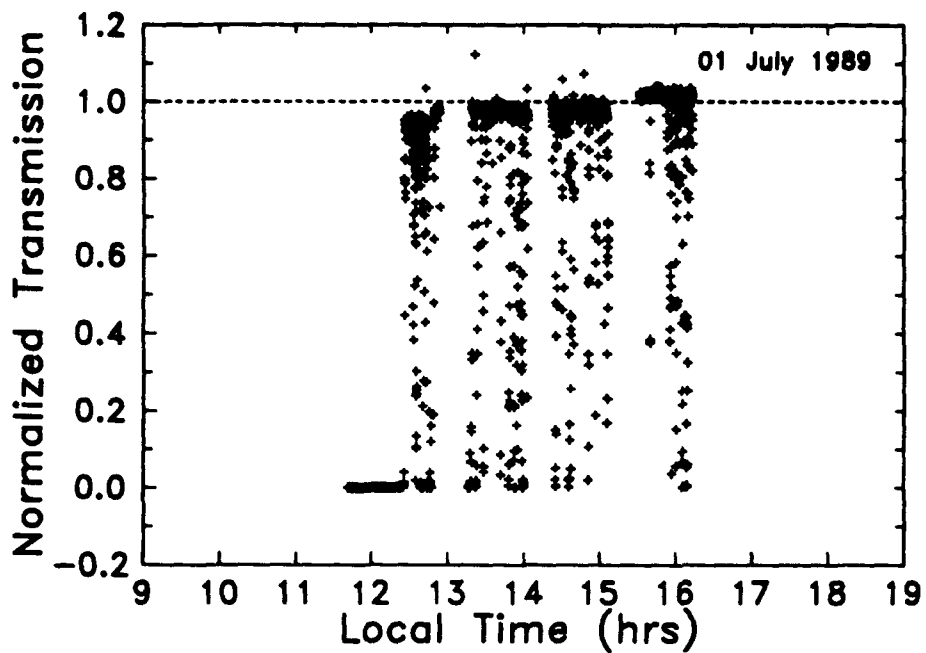


Figure 23. Values of Transmission as a Function of Time for 1 July 1989 After Removing Molecular, Aerosol, and Solar Zenith Effects

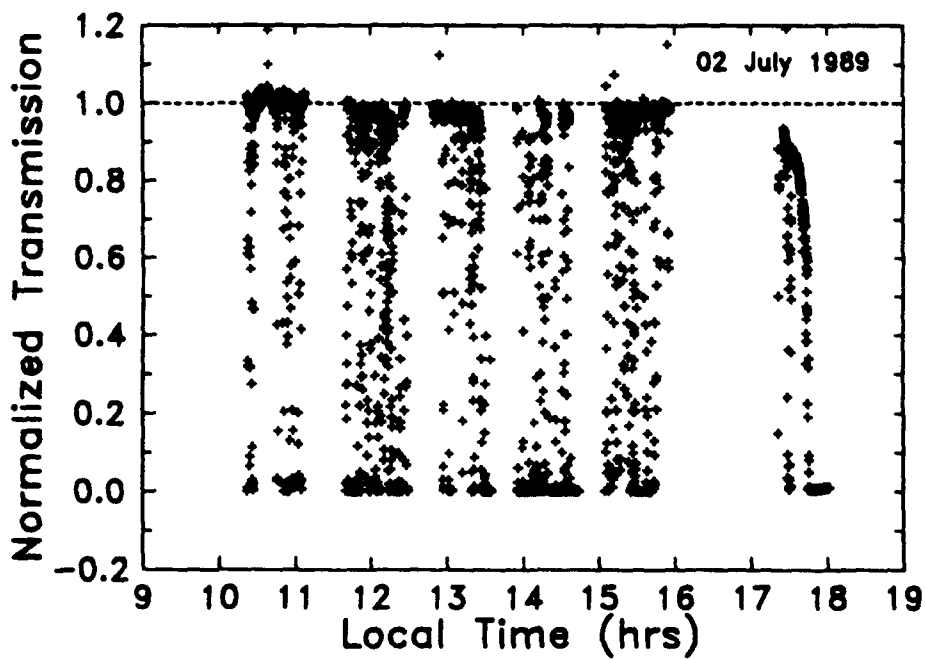


Figure 24. Values of Transmission as a Function of Time for 2 July 1989 After Removing Molecular, Aerosol, and Solar Zenith Effects

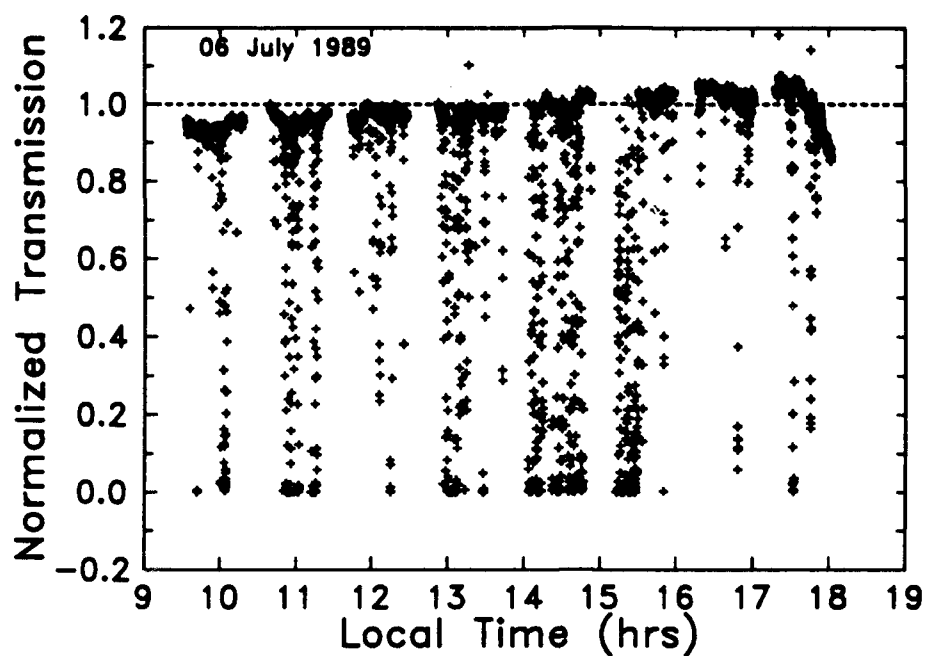


Figure 25. Values of Transmission as a Function of Time for 6 July 1989 After Removing Molecular, Aerosol, and Solar Zenith Effects

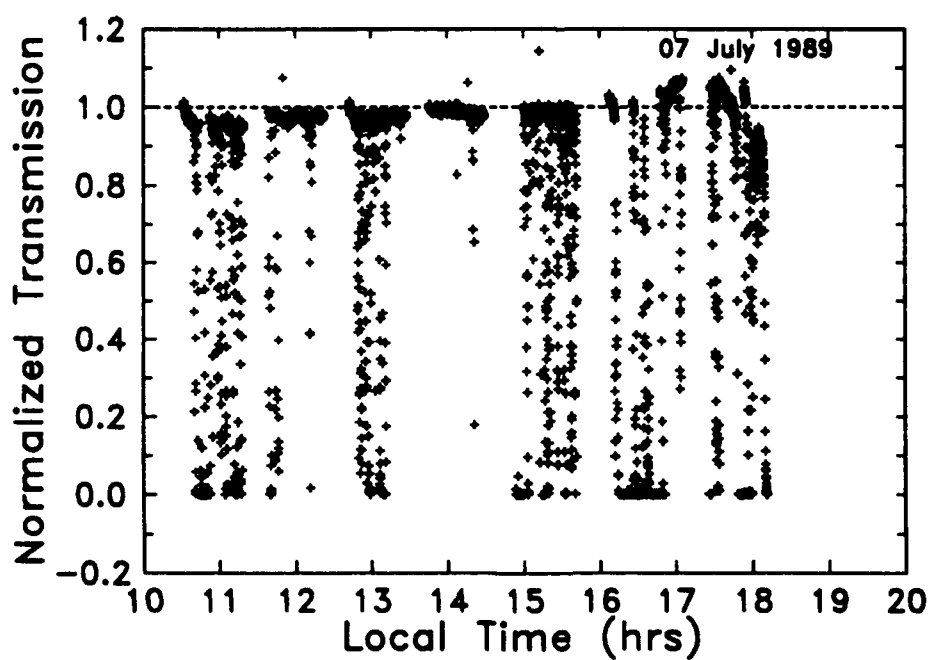


Figure 26. Values of Transmission as a Function of Time for 7 July 1989 After Removing Molecular, Aerosol, and Solar Zenith Effects

Table 4. Daily Occurrences of Inferred τ_{cld} as a Function of Transmission. For example, the first entry means that there were 206 data points of τ_{cld} between 0.0 and 0.1 on 25 June 1989 after aerosol, molecular, and zenith effects were removed

| # OF OCCURENCES | 25 JUNE | 28 JUNE | 1 JULY | 2 JULY | 6 JULY | 7 JULY |
|----------------------|---------|---------|--------|--------|--------|--------|
| τ_{cld} 0.0-0.1 | 206 | 247 | 414 | 1229 | 407 | 716 |
| τ_{cld} 0.1-0.2 | 8 | 21 | 21 | 44 | 76 | 69 |
| τ_{cld} 0.2-0.3 | 8 | 22 | 22 | 62 | 56 | 63 |
| τ_{cld} 0.3-0.4 | 21 | 29 | 29 | 48 | 51 | 59 |
| τ_{cld} 0.4-0.5 | 236 | 32 | 35 | 56 | 61 | 57 |
| τ_{cld} 0.5-0.6 | 213 | 39 | 25 | 73 | 62 | 68 |
| τ_{cld} 0.6-0.7 | 147 | 54 | 35 | 95 | 70 | 67 |
| τ_{cld} 0.7-0.8 | 37 | 112 | 44 | 135 | 95 | 91 |
| τ_{cld} 0.8-0.9 | 30 | 223 | 105 | 251 | 189 | 182 |
| τ_{cld} 0.9-1.0 | 284 | 1715 | 1760 | 1689 | 3968 | 3038 |

cirrus along the solar path, and values of τ_{cld} less than 0.1 represent conditions where the sun is fully obscured by clouds. With the exception of 25 June 1989, the number of occurrences of τ_{cld} as a function of τ_{cld} form a U-shaped distribution.

At this point, it is worth noting that surface observations from Ascension Island indicate the presence of cirrus for 25 June 1989. Additionally, the peak solar transmissions for 25 June 1989 are about 0.6 (see Figure 7), whereas peak solar transmissions on the five other days are closer to 0.8. Since the surface observations of visibility do not suggest any extreme aerosol loading on 25 June 1989, it is quite likely that cirrus are influencing all of the measurements on 25 June 1989. Moreover, the technique to remove aerosol and molecular effects is not adequate for 25 June 1989, so these data will be omitted from many of the analyses in this report. (Note that it is not easy to remove the contributions of cirrus because the thicknesses frequently vary.)

3.2 Discussion of Forward Scattering Effects

Before investigating the transmission properties of cloud gaps and thin spots, it was necessary to estimate how much the values of τ_{cld} were biased by forward scattering. (Note that for particles large compared with the wavelength, the extremely narrow forward lobes due to Fraunhofer diffraction cause additional radiation to be scattered into the instrument field-of-view.) To do this, correction factors for forward scattering were calculated using the model of Mill and Shettle⁵ and Fenn *et al.*⁶

⁵ Mill, J.D. and E.P. Shettle (1983) A Preliminary LOWTRAN Snow Model, AFGL-TR-83-0148, Hanscom AFB, MA, ADA129826.

⁶ Fenn, R.W., Clough, S.A., Gallery, W.O., Good, R.E., Kneizys, F.X., Mill, J.D., Rothman,

Briefly, in the Mill and Shettle model⁵, the relationship between the transmission measured by an instrument, τ_{inst} , and the true radiance transmission, τ_{true} , is given by

$$\tau_{inst} = \tau_{true}(1 + D \ln \tau_{true}). \quad (4)$$

The correction factor, D , is found by integrating the contributions from all of the space common to the beam and the receiver field-of-view. D depends on the half angle of the source, θ_s , the half angle of the receiver field-of-view, θ_o , and the particle size parameter, x , defined as the particle circumference divided by the wavelength of radiation. Fenn *et al.*⁶ have tabulated values of D in terms of the following two parameters:

$$\rho = \frac{\text{Max}(\theta_s, \theta_o)}{\text{Min}(\theta_s, \theta_o)} \quad (5)$$

and

$$v = x \text{Min}(\theta_s, \theta_o) \quad (6)$$

where *Max* and *Min* are, respectively, the larger and smaller of the arguments in parentheses.

For the solar transmissometer at Ascension Island, Table 5 lists the values of ρ and v for stratocumulus and cirrus clouds. When these values of ρ and v are used in the lookup table of Fenn *et al.*⁶, it is apparent that correction factors are less than 1% for stratocumulus clouds. Corrections for cirrus clouds are significant, however.

Table 5. Values of Parameters Used to Estimate the Effects of Forward Scattering on the Transmission Measurements at Ascension Island. The size parameters for stratocumulus and cirrus clouds represent typical particle radii of 5 and 100 μm , respectively

| PARAMETER | VALUE |
|---------------------|-------------|
| θ_o | 0.00123 rad |
| θ_s | 0.00465 rad |
| x (Stratocumulus) | 59.8 |
| x (Cirrus) | 1196.8 |
| ρ | 3.78 |
| v (Stratocumulus) | 0.0736 |
| v (Cirrus) | 1.472 |

L.S., Shettle, E.P., and Volz, F.E. (1985) Optical and Infrared Properties of the Atmosphere, Chapter 18 in *Handbook of Geophysics and the Space Environment*, A.S. Jursa Scientific Ed., Air Force Geophysics Laboratory, Hanscom AFB, MA, AFGL-TR-85-0315, ADA167000.

3.3 Cirrus Cloud Analysis

Physically, departures of the transmission values from 1.0 in Figures 21 through 26 represent cloud effects (*i.e.*, values of $\tau_{cl d} < 1.0$). Generally, the reduced transmissions are due to boundary layer stratocumulus clouds that frequently occur at Ascension Island. As noted in Section 3.1, however, the transmission data on 25 June 1989 are influenced by cirrus clouds. Although the technique to remove aerosol and molecular effects is not adequate for 25 June 1989, Figure 21 does show extended periods of partial transmission with very few times when it drops to 0.0 or rises to 1.0. Such behavior is characteristic of a fairly uniform cirrus sheet, rather than patchy stratocumulus.

In order to estimate cirrus transmissions, the measured transmissions for 25 June 1989 are compared against those from the other five days. Specifically, the departures from representative transmissions on "non cirrus" days are assumed to be the cirrus transmissions. In this analysis, which uses transmission data before aerosol and molecular effects were removed (see Figures 7 through 12), a detailed quantitative assessment is unwarranted because there are too many uncertainties, such as day-to-day variations of aerosol loading in the boundary layer and forward scattering effects (see Section 3.2). Furthermore, the analysis only considers the transmission envelopes for each day because departures from it are probably due to stratocumulus clouds.

Table 6 gives estimated cirrus transmissions on 25 June 1989 for each period when the solar transmissometer was operated. Note that the estimated cirrus equals the values on 25 June 1989 divided by those on "non cirrus" days. Also, note that transmissions on the "non cirrus" days all equal 0.75 because zenith angle effects are not too prevalent during these times. Table 6 suggests that cirrus transmissions are between about 0.40 and 0.80.

Table 6. Estimated Cirrus Transmissions on 25 June 1989. Values are derived from measured solar measurements on 25 June 1989 and representative transmissions for "non cirrus" days which are also shown

| TIME (Local) | Transmission on 25 JUNE 1989 | Transmission on Non Cirrus Days | Estimated Cirrus Transmission |
|-----------------|---------------------------------|------------------------------------|----------------------------------|
| 11:43-12:01 | 0.60 | 0.75 | 0.80 |
| 12:19-12:36 | 0.55 | 0.75 | 0.73 |
| 12:54-13:11 | 0.30 | 0.75 | 0.40 |
| 13:29-13:46 | 0.35 | 0.75 | 0.47 |
| 14:05-14:22 | 0.30 | 0.75 | 0.40 |

Given cirrus transmissions between 0.40 and 0.80, the corresponding cirrus cloud depths were estimated using the standard LOWTRAN7 cirrus cloud model⁷. To do this, cirrus cloud transmission in the direction of the sun was calculated as a function of solar zenith angle and cloud thickness. The calculations were performed using the default cloud base height of 10 km and the default extinction coefficient of 0.14 km^{-1} for a wavelength $0.55 \mu\text{m}$. (Note that the base altitude is not important in these calculations because cirrus transmission does not depend on the base altitude.) For reference, the calculated cirrus transmissions are shown in Figure 27. The data in Figure 27 were then mapped on to the local time grid for Ascension Island (see Figure 28). To estimate cirrus cloud thicknesses over Ascension Island, the values of τ_{cld} for 25 June 1989 (see Figure 21) were then compared against the transmission curves in Figure 28. Specifically, an estimate of cirrus cloud thickness was given by the transmission curve having transmission values that best matched the values of τ_{cld} when cirrus clouds were suspected. For the times between 1300 and 1430 hrs on 25 June 1989, cirrus cloud thicknesses are estimated to be between 1.0 and 2.2 km. These estimates are plausible, and they are consistent with cirrus observations from aircraft for 25 June 1989.

3.4 Stratocumulus Cloud Analysis

The stratocumulus clouds observed over Ascension Island are similar to those generally found in trade wind environments. Individual clouds are often quite small and their distribution is rather regular, so that a group of stratocumulus clouds develops a checkerboard appearance when viewed from above. From the ground, stratocumulus clouds are whitish or grayish with dark spots.

The current analysis focuses on the properties of cloud edges and thin spots in stratocumulus clouds. These properties are of interest to those who model radiative transfer in climate studies. For the solar transmissometer measurements, stratocumulus cloud edges and thin spots are probable whenever values of τ_{cld} are between 0.1 and 0.9.

3.4.1 Thickness Estimates of Cloud Edges and Thin Spots

The depths of thin spots and cloud edges of stratocumulus clouds were estimated using the cloud models in LOWTRAN7. To do this, transmission through a stratocumulus cloud in the direction of the sun was calculated as a function of solar zenith angle and cloud thickness. Here, the standard LOWTRAN7 profile of liquid water content (and hence number density profile) was used in the simulation of stratocumulus clouds of different depths. For reference, the calculated transmissions are shown in Figure 29. The values in Figure 29 were then mapped on to the local time grid for Ascension Island (see Figure 30). Figure 30 was then examined to see what transmission curves produced transmissions between 0.1 and 0.9 for most daylight hours. Figure 30 suggests that cloud depths of 5 to 50 m are required to give values of τ_{cld} between 0.1 and 0.9. However, these depths are probably underestimates because thin spots and cloud edges often result from reduced number density profiles rather than reduced cloud thickness alone.

⁷ Shettle, E.P. (1989) "Models of Aerosols, Clouds, and Precipitation for Atmospheric Propagation Studies", Proceedings of the AGARD 45th Symposium of the Electromagnetic Wave Propagation Panel on *Atmospheric Propagation in the UV, Visible, IR, and mm-Wave Region and Related System Aspects*, Copenhagen, Denmark, 9-13 October 1989.

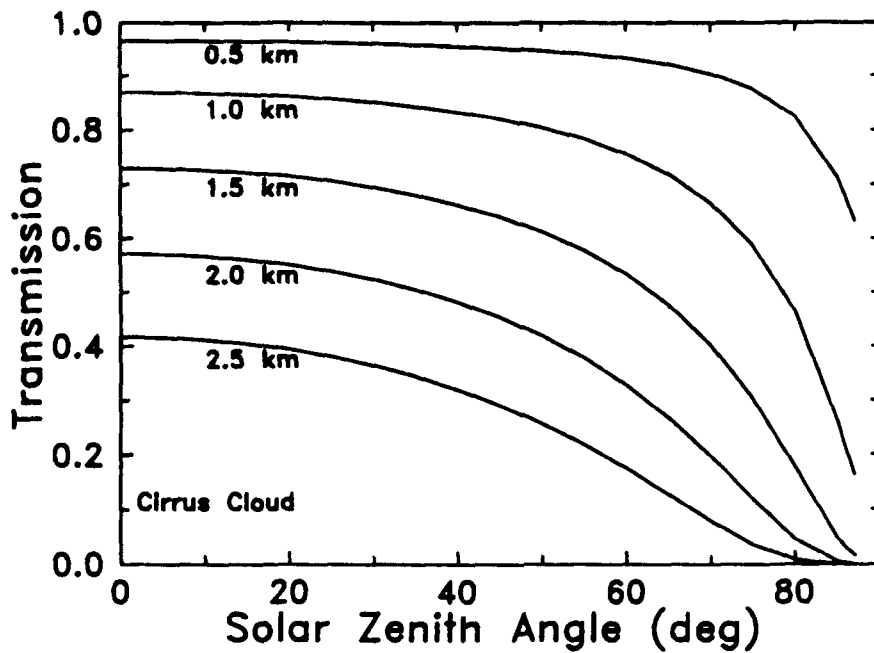


Figure 27. Calculated Transmission Through Cirrus Clouds in the Solar Direction Versus Solar Zenith Angle for Cloud Thicknesses of 0.5, 1.0, 1.5, 2.0, and 2.5 km. Note that these transmissions are for the cirrus alone, and they do not include effects from aerosol and molecules within the cirrus

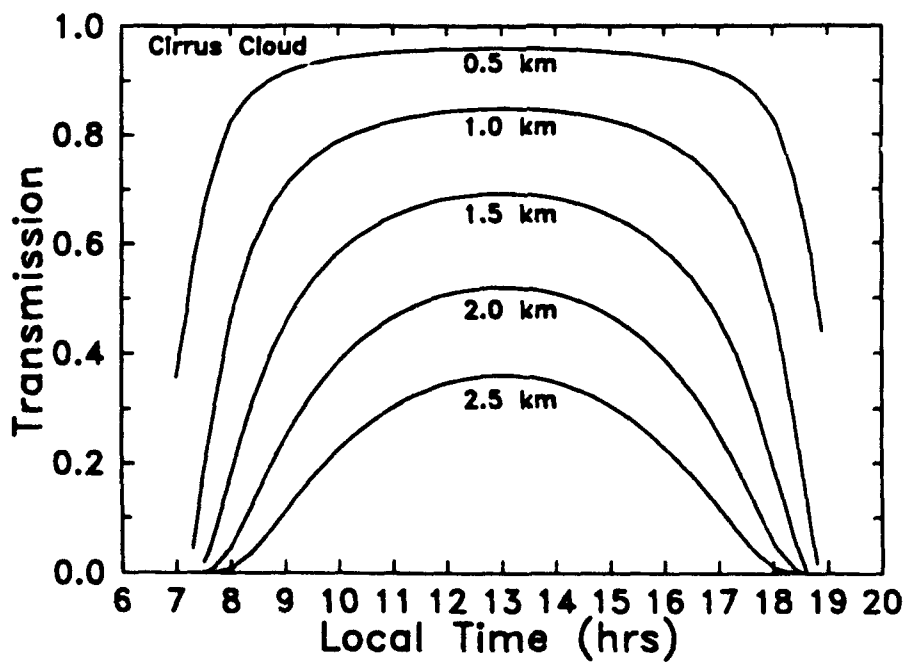


Figure 28. Calculated Transmission Through Cirrus Clouds in the Solar Direction Versus Local Time for Ascension Island for Cloud Thicknesses of 0.5, 1.0, 1.5, 2.0, and 2.5 km. Note that these transmissions are for the cirrus alone, and they do not include effects from aerosol and molecules within the cirrus

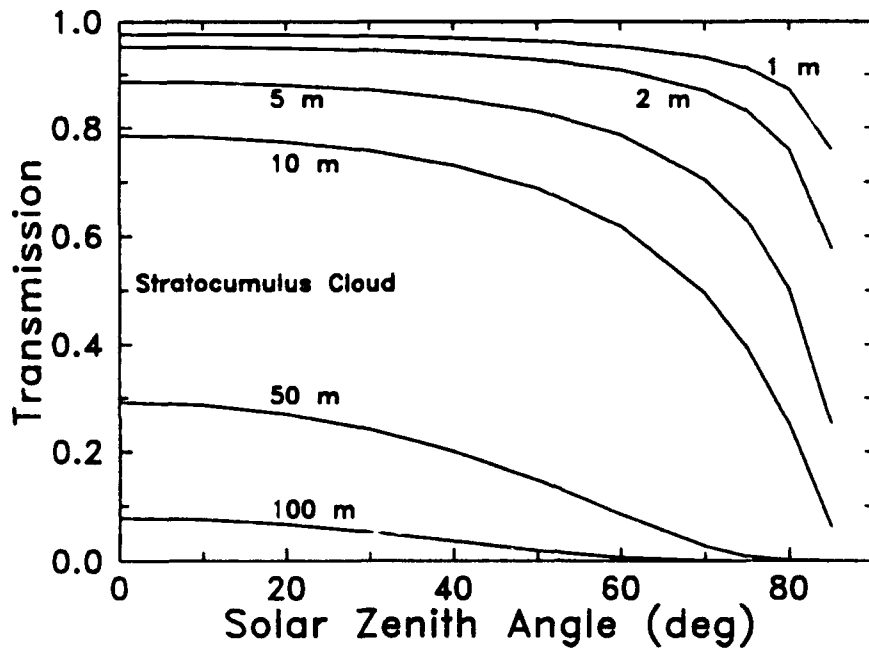


Figure 29. Calculated Transmission Through Stratocumulus Clouds in the Solar Direction Versus Solar Zenith Angle for Cloud Thicknesses of 1, 2, 5, 10, 50, and 100 m. Note that these transmissions are for the stratocumulus alone, and they do not include effects from aerosol and molecules within the stratocumulus

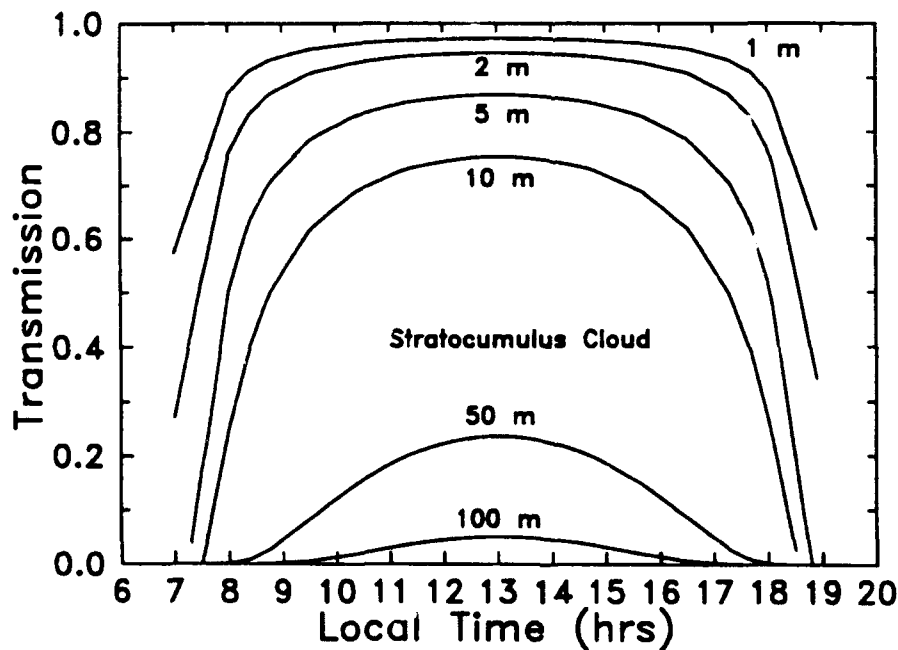


Figure 30. Calculated Transmission Through Stratocumulus Clouds in the Solar Direction Versus Local Time for Ascension Island for Cloud Thicknesses of 1, 2, 5, 10, 50, and 100 m. Note that these transmissions are for the stratocumulus alone, and they do not include effects from aerosol and molecules within the stratocumulus

3.4.2 Occurrence of Cloud Edges and Thin Spots

This section examines the frequency of occurrence of individual transmission measurements in which cloud edges and thin spots are suspected. Initially, the analysis only considered values of τ_{cld} between 0.1 and 0.9. Here, the rationale was that cloud edges and thin spots may exhibit some behavior that was independent of day-to-day fluctuations in average cloud cover. For example, Table 7 shows the daily percent distributions of individual measurements of cloud transmission in which only presumed occurrences of cloud thin spots and edges have been included. These percent distributions were derived from the data in Table 4 so that the first entry in Table 7 represents

$$100 \times \frac{8}{(8 + 8 + 21 + 236 + 213 + 147 + 37 + 30)} = 2.54\%. \quad (7)$$

Except for 25 June 1989, the data seem to show the same trends. That is, there is a uniform distribution of transmission values between about 0.1 and 0.7. Also, the percentages increase significantly as transmissions increase from 0.7 to 0.9. This is interesting because it indicates that the stratocumulus have very similar edge characteristics from day-to-day. However, note that the percent distributions for 25 June 1989 deviate from these generalizations because of cirrus clouds. Figure 31 shows these cloud statistics in pictorial form.

Table 7. Daily Percent Distributions of Individual Transmission Measurements In Which Only Presumed Occurrences of Cloud Edges and Thin Spots Have Been Included. For example, the first entry means that on 25 June 1989, 2.54% of all presumed cloud edge and thin spot measurements were between 0.1 and 0.2

| % OF OCCURRENCES | 25 JUNE | 28 JUNE | 1 JULY | 2 JULY | 6 JULY | 7 JULY |
|----------------------|---------|---------|--------|--------|--------|--------|
| τ_{cld} 0.1-0.2 | 2.54 | 3.95 | 6.65 | 5.76 | 11.52 | 10.52 |
| τ_{cld} 0.2-0.3 | 1.13 | 4.14 | 6.96 | 8.12 | 8.48 | 9.60 |
| τ_{cld} 0.3-0.4 | 2.96 | 5.45 | 9.18 | 6.28 | 7.73 | 8.99 |
| τ_{cld} 0.4-0.5 | 33.24 | 6.02 | 11.08 | 7.33 | 9.24 | 8.69 |
| τ_{cld} 0.5-0.6 | 30.00 | 7.33 | 7.91 | 9.55 | 9.39 | 10.37 |
| τ_{cld} 0.6-0.7 | 20.70 | 10.15 | 11.08 | 12.43 | 10.61 | 10.21 |
| τ_{cld} 0.7-0.8 | 5.21 | 21.05 | 13.92 | 17.67 | 14.39 | 13.87 |
| τ_{cld} 0.8-0.9 | 4.23 | 41.92 | 33.23 | 32.85 | 28.64 | 27.74 |

Table 8 shows daily averages and standard deviations of cloud transmissions in which only presumed occurrences of cloud thin spots and edges have been included. The table suggests that the averages and standard deviations for 1, 2, 6, and 7 July 1989 are remarkably similar, although the average and standard deviation are, respectively, a little higher and lower for 28 June 1989. However, the results for 25 June 1989 clearly differ from the other days because of the presence of cirrus clouds.

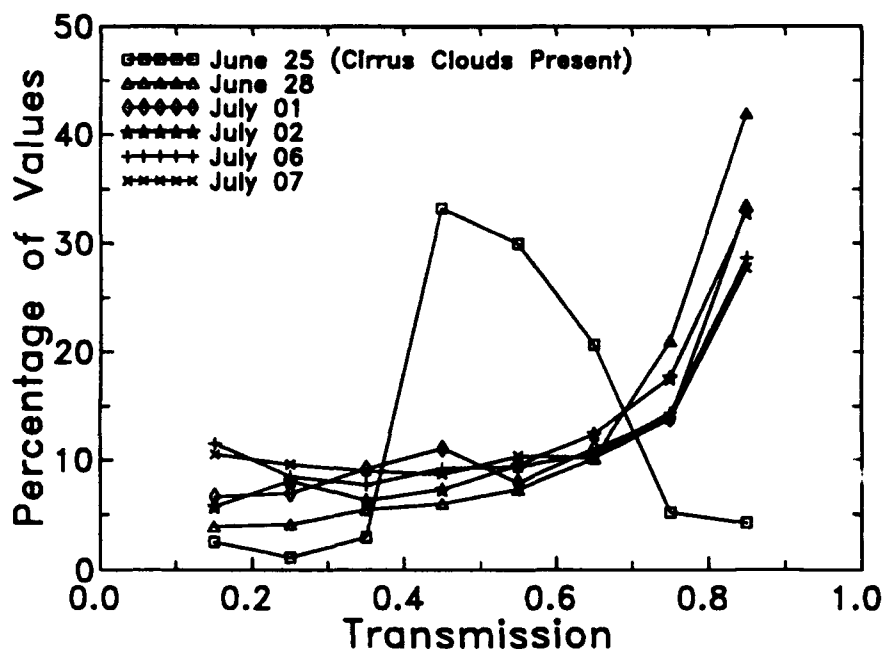


Figure 31. Daily Percent Distributions of Individual Transmission Measurements In Which Only Presumed Occurrences of Cloud Edges and Thin Spots Have Been Included

Table 8. Daily Averages and Standard Deviations of Transmission In Which Only Presumed Occurrences of Cloud Thin Spots and Edges Have Been Included

| | 25 JUNE | 28 JUNE | 1 JULY | 2 JULY | 6 JULY | 7 JULY |
|--|---------|---------|--------|--------|--------|--------|
| TOTAL POINTS | 1200 | 2494 | 2490 | 3682 | 5035 | 4410 |
| EDGE POINTS (0.1 < τ_{cld} < 0.9) | 710 | 532 | 316 | 764 | 660 | 656 |
| AVERAGE OF EDGE POINTS | 0.5439 | 0.6851 | 0.6132 | 0.6309 | 0.5813 | 0.5765 |
| ST DEV OF EDGE POINTS | 0.1300 | 0.2061 | 0.2369 | 0.2312 | 0.2567 | 0.2512 |

Values of τ_{cld} were then used to estimate the overall opacity of stratocumulus clouds over Ascension Island. To do this, the number of occurrences of cloud thin spots and edges, N_{edge} , were compared against the total number of cloud occurrences which is given by

$$N_{edge} + N_{cld} \quad (8)$$

where N_{cld} equals the number of occurrences in which the clouds were opaque (i.e., values of τ_{cld} less than 0.1). In general terms, the ratio of $N_{edge}/(N_{edge} + N_{cld})$ gives a measure of overall cloud opacity. Values closer to 1.0 suggest that the clouds possess many thin spots and values closer to 0.0 suggest that most of the clouds are opaque. Table 9 gives daily

values of $N_{edge}/(N_{edge} + N_{cld})$ at Ascension Island. (Because of the presence of cirrus clouds, data for 25 June 1989 were not included in these estimates.) In Table 9, the daily values of $N_{edge}/(N_{edge} + N_{cld})$ vary somewhat probably because they are influenced by biases from the daily average cloud cover. However, the fact that daily values of $N_{edge}/(N_{edge} + N_{cld})$ are much greater than 0.0 means stratocumulus clouds over Ascension Island often are not opaque, and they frequently transmit partial solar radiation. Since stratocumulus clouds often cover broad regions of the marine environment, these findings could be of interest to climate modeling studies which often assume stratocumulus clouds to be fully opaque.

Table 9. Daily Values of $N_{edge}/(N_{edge} + N_{cld})$ for Over Ascension Island. Note that this ratio gives an estimate of cloud opacity. A value close to 1.0 means that the clouds possess many thin spots and values closer to 0.0 suggest that most of the clouds are opaque.

| | 28 JUNE | 1 JULY | 2 JULY | 6 JULY | 7 JULY |
|--|---------|--------|--------|--------|--------|
| NO. OF EDGE PTS, N_{edge} | 532 | 316 | 764 | 660 | 656 |
| NO. OF OPAQUE PTS, N_{cld} | 247 | 414 | 1229 | 407 | 716 |
| TOTAL CLOUD PTS | 779 | 730 | 1993 | 1067 | 1372 |
| $N_{edge}/(N_{edge} + N_{cld})$ | 0.6829 | 0.4328 | 0.3833 | 0.6185 | 0.4781 |

3.4.3 Time Duration of Cloud Edges and Thin Spots

This section examines the time duration of cloud edges and thin spots. In the analysis, daily time series of τ_{cld} were subdivided into continuously distinct time periods in which:

1. Skies were clear in the direction of the sun
2. Clouds fully blocked the sun
3. Cloud edges and thin spots dominated.

In order to be classified as a "clear" period, values of τ_{cld} had to be greater than 0.9 for at least 60 seconds. Similarly, a fully "cloudy" period was assigned whenever values of τ_{cld} were less than 0.1 for at least 60 seconds. All remaining time periods in the τ_{cld} time series were classified as being dominated by cloud edges and thin spots. Note in this simple classification scheme that a given cloud edge and thin spot event can contain values of τ_{cld} less than 0.1 or greater than 0.9, provided they are of short duration. Here, the rationale is that cloud edges and thin spots often exhibit a high degree of variability and, therefore, some limiting values would be expected. Also, the 60 second criteria for fully clear and cloudy events was chosen without any true scientific basis; rather, it is based on human experience.

For reference, Tables 10 through 14 show, respectively, the time periods and durations when cloud edges and thin spots occurred on 28 June, 1, 2, 6, and 7 July 1989. (Once again, data for 25 June 1989 were not included in this analysis because of cirrus clouds.) Note that the minimum duration is four seconds which equals the transmission measurement spacing. The

duration of cloud edges and thin spot events were then grouped into evenly spaced time bins and the frequencies of occurrence were tabulated (see Table 15). Figure 32 presents these occurrences in a histogram form. The results suggest that for Ascension Island, time durations of most cloud edges and thin spot events are less than 200 seconds, although some events exceed 250 seconds. The distribution is not gaussian; rather, events of less than 60 seconds occur most frequently and there is a gradual falloff in the number of occurrences as the time durations become longer. However, the results may suggest a local peak around 40 seconds given that the number of events less than 10 seconds may be influenced by spurious measurements with the transmissometer.

Table 10. Times and Durations of Presumed Cloud Edges and Thin Spots for 28 June 1989 at Ascension Island

| START TIME (Local) | END TIME (Local) | DURATION (sec) |
|-----------------------|---------------------|-------------------|
| 13.5245 | 13.5488 | 92 |
| 13.5878 | 13.5878 | 4 |
| 13.6255 | 13.6255 | 4 |
| 13.6833 | 13.6988 | 60 |
| 13.7422 | 13.7678 | 96 |
| 13.8112 | 13.8267 | 60 |
| 13.8955 | 13.9000 | 20 |
| 13.9222 | 13.9288 | 28 |
| 13.9588 | 14.0067 | 176 |
| 14.0512 | 14.1000 | 180 |
| 14.1312 | 14.1422 | 44 |
| 14.1722 | 14.1812 | 36 |
| 14.2200 | 14.2322 | 48 |
| 14.4533 | 14.4533 | 4 |
| 14.5955 | 14.6055 | 40 |
| 14.6222 | 14.6222 | 4 |
| 14.6555 | 14.6755 | 76 |
| 14.7233 | 14.7667 | 160 |
| 14.8922 | 14.9245 | 120 |
| 15.0188 | 15.0388 | 76 |
| 15.0667 | 15.0688 | 12 |
| 15.1500 | 15.1600 | 40 |
| 15.7367 | 15.7367 | 4 |
| 16.3878 | 16.4788 | 332 |
| 16.5578 | 16.6200 | 228 |
| 16.7422 | 16.8112 | 252 |
| 16.8388 | 16.9800 | 512 |
| 17.4145 | 17.4233 | 36 |
| 17.4467 | 17.4778 | 116 |
| 17.5167 | 17.5488 | 120 |

Table 11. Times and Durations of Presumed Cloud Edges and Thin Spots for 1 July 1989 at Ascension Island

| START TIME (Local) | END TIME (Local) | DURATION (sec) |
|-----------------------|---------------------|-------------------|
| 12.4267 | 12.4355 | 36 |
| 12.5300 | 12.5955 | 240 |
| 12.6288 | 12.6367 | 32 |
| 12.6600 | 12.7455 | 312 |
| 12.7745 | 12.7933 | 72 |
| 12.8100 | 12.8255 | 60 |
| 12.8945 | 12.8955 | 8 |
| 13.3112 | 13.3212 | 40 |
| 13.3722 | 13.3933 | 80 |
| 13.4455 | 13.4455 | 4 |
| 13.4633 | 13.4767 | 52 |
| 13.5078 | 13.5112 | 16 |
| 13.5878 | 13.5878 | 4 |
| 13.6900 | 13.6978 | 32 |
| 13.7978 | 13.8245 | 100 |
| 13.8588 | 13.8712 | 48 |
| 13.8978 | 13.9200 | 84 |
| 13.9533 | 13.9833 | 112 |
| 14.0012 | 14.0022 | 8 |
| 14.0388 | 14.0467 | 32 |
| 14.3733 | 14.3767 | 16 |
| 14.4100 | 14.4388 | 108 |
| 14.5022 | 14.5067 | 20 |
| 14.5312 | 14.5312 | 4 |
| 14.5633 | 14.5633 | 4 |
| 14.5878 | 14.6278 | 148 |
| 14.6545 | 14.6600 | 24 |
| 14.7500 | 14.7500 | 4 |
| 14.8478 | 14.8645 | 64 |
| 14.9433 | 14.9488 | 24 |
| 14.9788 | 14.9812 | 12 |
| 15.0000 | 15.0012 | 8 |
| 15.0645 | 15.0645 | 4 |
| 15.0922 | 15.1122 | 76 |
| 15.6600 | 15.6645 | 20 |
| 15.8867 | 15.8867 | 4 |
| 15.9245 | 15.9500 | 96 |
| 16.0022 | 16.0300 | 104 |
| 16.0533 | 16.0545 | 8 |
| 16.0855 | 16.0900 | 20 |
| 16.1145 | 16.1755 | 224 |

Table 12. Times and Durations of Presumed Cloud Edges and Thin Spots for 2 July 1989 at Ascension Island

| START TIME (Local) | END TIME (Local) | DURATION (sec) |
|-----------------------|---------------------|-------------------|
| 10.3622 | 10.3767 | 56 |
| 10.3945 | 10.4633 | 252 |
| 10.7555 | 10.7655 | 40 |
| 10.8345 | 10.9012 | 244 |
| 10.9233 | 10.9322 | 36 |
| 10.9567 | 10.9733 | 64 |
| 10.9933 | 10.9955 | 12 |
| 11.0345 | 11.0922 | 212 |
| 11.6655 | 11.6978 | 120 |
| 11.7322 | 11.7533 | 80 |
| 11.8000 | 11.8012 | 8 |
| 11.8212 | 11.8322 | 44 |
| 11.8555 | 11.8955 | 148 |
| 11.9455 | 11.9778 | 120 |
| 11.9945 | 12.0000 | 24 |
| 12.0522 | 12.0600 | 32 |
| 12.0967 | 12.1433 | 172 |
| 12.1612 | 12.2400 | 288 |
| 12.2622 | 12.2855 | 88 |
| 12.3022 | 12.3078 | 24 |
| 12.3778 | 12.3822 | 20 |
| 12.4133 | 12.4145 | 8 |
| 12.4345 | 12.4378 | 16 |
| 12.4612 | 12.4812 | 76 |
| 12.9412 | 12.9622 | 80 |
| 12.9800 | 12.9822 | 12 |
| 13.0145 | 13.0267 | 48 |
| 13.0945 | 13.1055 | 44 |
| 13.2012 | 13.2088 | 32 |
| 13.2955 | 13.3655 | 256 |
| 13.4200 | 13.4622 | 156 |
| 13.4945 | 13.5133 | 72 |
| 13.5733 | 13.5833 | 40 |
| 13.9122 | 13.9333 | 80 |
| 13.9912 | 14.0000 | 36 |
| 14.0745 | 14.0922 | 68 |
| 14.1288 | 14.1400 | 44 |
| 14.1778 | 14.1788 | 8 |
| 14.2133 | 14.2678 | 200 |
| 14.2878 | 14.2933 | 24 |

Table 12. (cont.)

| START TIME | END TIME | DURATION |
|-------------------|-----------------|-----------------|
| (Local) | (Local) | (sec) |
| 14.3155 | 14.3433 | 104 |
| 14.4245 | 14.4333 | 36 |
| 14.5155 | 14.5233 | 32 |
| 14.5433 | 14.5555 | 48 |
| 14.5745 | 14.6078 | 124 |
| 15.0788 | 15.0788 | 4 |
| 15.0888 | 15.1212 | 120 |
| 15.1712 | 15.2433 | 264 |
| 15.2745 | 15.2855 | 44 |
| 15.3033 | 15.3400 | 136 |
| 15.3778 | 15.4133 | 132 |
| 15.4355 | 15.5088 | 268 |
| 15.5912 | 15.5912 | 4 |
| 15.6167 | 15.6388 | 84 |
| 15.6945 | 15.6945 | 4 |
| 15.7222 | 15.7378 | 60 |
| 15.7545 | 15.7655 | 44 |
| 15.8055 | 15.8100 | 20 |
| 15.9122 | 15.9288 | 64 |
| 17.3545 | 17.3633 | 36 |
| 17.3722 | 17.3788 | 28 |
| 17.4422 | 17.4912 | 180 |

Table 13. Times and Durations of Presumed Cloud Edges and Thin Spots for 6 July 1989 at Ascension Island

| START TIME (Local) | END TIME (Local) | DURATION (sec) |
|-----------------------|---------------------|-------------------|
| 9.5912 | 9.5912 | 4 |
| 9.7045 | 9.7055 | 8 |
| 9.8167 | 9.8278 | 44 |
| 9.8922 | 9.9088 | 64 |
| 9.9412 | 9.9412 | 4 |
| 9.9845 | 10.0588 | 272 |
| 10.0767 | 10.0867 | 40 |
| 10.2088 | 10.2088 | 4 |
| 10.7012 | 10.7022 | 8 |
| 10.7345 | 10.7388 | 20 |
| 10.8255 | 10.8633 | 140 |
| 10.8822 | 10.9022 | 76 |
| 10.9278 | 10.9888 | 224 |
| 11.0145 | 11.0422 | 104 |
| 11.1988 | 11.2000 | 8 |
| 11.2212 | 11.2867 | 240 |
| 11.7588 | 11.7633 | 20 |
| 11.8288 | 11.8300 | 8 |
| 11.8500 | 11.8500 | 4 |
| 11.9700 | 11.9733 | 16 |
| 12.0078 | 12.0112 | 16 |
| 12.0522 | 12.0600 | 32 |
| 12.0945 | 12.1212 | 100 |
| 12.2400 | 12.2700 | 112 |
| 12.4178 | 12.4200 | 12 |
| 12.9078 | 12.9422 | 128 |
| 12.9667 | 13.0112 | 164 |
| 13.0688 | 13.0878 | 72 |
| 13.1245 | 13.1700 | 168 |
| 13.1822 | 13.1845 | 12 |
| 13.2278 | 13.2500 | 84 |
| 13.2678 | 13.2800 | 48 |
| 13.3033 | 13.3033 | 4 |
| 13.3633 | 13.3633 | 4 |
| 13.4600 | 13.4600 | 4 |
| 13.4800 | 13.4912 | 44 |
| 13.7100 | 13.7178 | 32 |
| 14.0533 | 14.0622 | 36 |

Table 13. (cont.)

| START TIME (Local) | END TIME (Local) | DURATION (sec) |
|-----------------------|---------------------|-------------------|
| 14.0912 | 14.1288 | 140 |
| 14.1467 | 14.1745 | 104 |
| 14.2078 | 14.2100 | 12 |
| 14.2188 | 14.2512 | 120 |
| 14.3645 | 14.3755 | 44 |
| 14.4300 | 14.4578 | 104 |
| 14.4855 | 14.5455 | 220 |
| 14.5633 | 14.5633 | 4 |
| 14.5800 | 14.6367 | 208 |
| 14.6578 | 14.6622 | 20 |
| 14.6800 | 14.7267 | 172 |
| 14.7455 | 14.7512 | 24 |
| 14.7745 | 14.7745 | 4 |
| 14.8755 | 14.8855 | 40 |
| 15.2078 | 15.2645 | 208 |
| 15.3178 | 15.3678 | 184 |
| 15.4088 | 15.4512 | 156 |
| 15.4688 | 15.5033 | 128 |
| 15.5488 | 15.5600 | 44 |
| 15.7122 | 15.7155 | 16 |
| 15.8288 | 15.8378 | 36 |
| 15.8888 | 15.8900 | 8 |
| 16.3167 | 16.3300 | 52 |
| 16.6367 | 16.6378 | 8 |
| 16.7967 | 16.8078 | 44 |
| 16.8322 | 16.8333 | 8 |
| 16.9433 | 16.9467 | 16 |
| 17.5122 | 17.5267 | 56 |
| 17.5445 | 17.5488 | 20 |
| 17.7388 | 17.7645 | 96 |
| 17.8222 | 17.8345 | 48 |

Table 14. Times and Durations of Presumed Cloud Edges and Thin Spots for 7 July 1989 at Ascension Island

| START TIME (Local) | END TIME (Local) | DURATION (sec) |
|-----------------------|---------------------|-------------------|
| 10.6678 | 10.7245 | 208 |
| 10.7633 | 10.7733 | 40 |
| 10.8100 | 10.8133 | 16 |
| 10.8522 | 10.8522 | 4 |
| 10.8833 | 10.8922 | 36 |
| 10.9112 | 10.9178 | 28 |
| 10.9488 | 10.9500 | 8 |
| 10.9845 | 11.0412 | 208 |
| 11.0878 | 11.1045 | 64 |
| 11.1667 | 11.2100 | 160 |
| 11.2345 | 11.2533 | 72 |
| 11.2712 | 11.3200 | 180 |
| 11.6478 | 11.6812 | 124 |
| 11.7345 | 11.7433 | 36 |
| 11.7633 | 11.7788 | 60 |
| 12.1888 | 12.2200 | 116 |
| 12.8233 | 12.8855 | 228 |
| 12.9245 | 12.9800 | 204 |
| 13.0022 | 13.0055 | 16 |
| 13.0345 | 13.0378 | 16 |
| 13.0578 | 13.0612 | 16 |
| 13.1088 | 13.1278 | 72 |
| 13.1545 | 13.1555 | 8 |
| 13.1878 | 13.2033 | 60 |
| 14.1322 | 14.1322 | 4 |
| 14.3388 | 14.3578 | 72 |
| 15.0088 | 15.0122 | 16 |
| 15.0378 | 15.0667 | 108 |
| 15.0845 | 15.0855 | 8 |
| 15.1300 | 15.1378 | 32 |
| 15.1722 | 15.1733 | 8 |
| 15.2122 | 15.2312 | 72 |
| 15.2812 | 15.3800 | 360 |
| 15.4455 | 15.4788 | 124 |
| 15.5067 | 15.5088 | 12 |
| 15.5312 | 15.5855 | 200 |
| 15.6088 | 15.6445 | 132 |

Table 14. (cont.)

| START TIME (Local) | END TIME (Local) | DURATION (sec) |
|-------------------------------------|-----------------------------------|---------------------------------|
| 15.6645 | 15.7033 | 144 |
| 16.1988 | 16.2255 | 100 |
| 16.2378 | 16.2388 | 8 |
| 16.4367 | 16.4822 | 168 |
| 16.5588 | 16.5688 | 40 |
| 16.5800 | 16.5978 | 68 |
| 16.6212 | 16.6478 | 100 |
| 16.8200 | 16.8345 | 56 |
| 16.8612 | 16.8812 | 76 |
| 17.0578 | 17.0945 | 136 |
| 17.4633 | 17.4912 | 104 |
| 17.5155 | 17.5655 | 184 |
| 17.7667 | 17.7688 | 12 |
| 17.7955 | 17.8078 | 48 |
| 17.8955 | 17.9455 | 184 |
| 17.9688 | 17.9833 | 56 |
| 18.0012 | 18.0733 | 264 |

Table 15. Frequency of Occurrence of Cloud Edges and Thin Spots Events of Different Time Durations. The daily averages and standard deviations for the time durations are also listed

| # OF EVENTS | 28 JUNE | 1 JULY | 2 JULY | 6 JULY | 7 JULY |
|--------------------------------|----------------|---------------|---------------|---------------|---------------|
| TOTAL | 30 | 41 | 62 | 69 | 54 |
| < 10 sec EVENTS | 5 | 11 | 6 | 16 | 7 |
| 10-30 sec EVENTS | 3 | 8 | 9 | 12 | 8 |
| 30-50 sec EVENTS | 6 | 6 | 16 | 13 | 6 |
| 50-70 sec EVENTS | 2 | 3 | 5 | 3 | 6 |
| 70-90 sec EVENTS | 2 | 4 | 7 | 3 | 5 |
| 90-110 sec EVENTS | 2 | 4 | 1 | 5 | 4 |
| 110-130 sec EVENTS | 3 | 1 | 4 | 4 | 3 |
| 130-150 sec EVENTS | 0 | 1 | 3 | 2 | 3 |
| 150-170 sec EVENTS | 1 | 0 | 1 | 3 | 2 |
| 170-190 sec EVENTS | 2 | 0 | 2 | 2 | 3 |
| 190-210 sec EVENTS | 0 | 0 | 1 | 2 | 4 |
| > 210 sec EVENTS | 4 | 3 | 7 | 4 | 3 |
| AVE TIME OF EDGE EVENTS | 98.6 | 56.2 | 83.5 | 67.1 | 89.3 |
| STD DEV OF EDGE EVENTS | 106.1 | 63.7 | 73.5 | 64.2 | 73.8 |

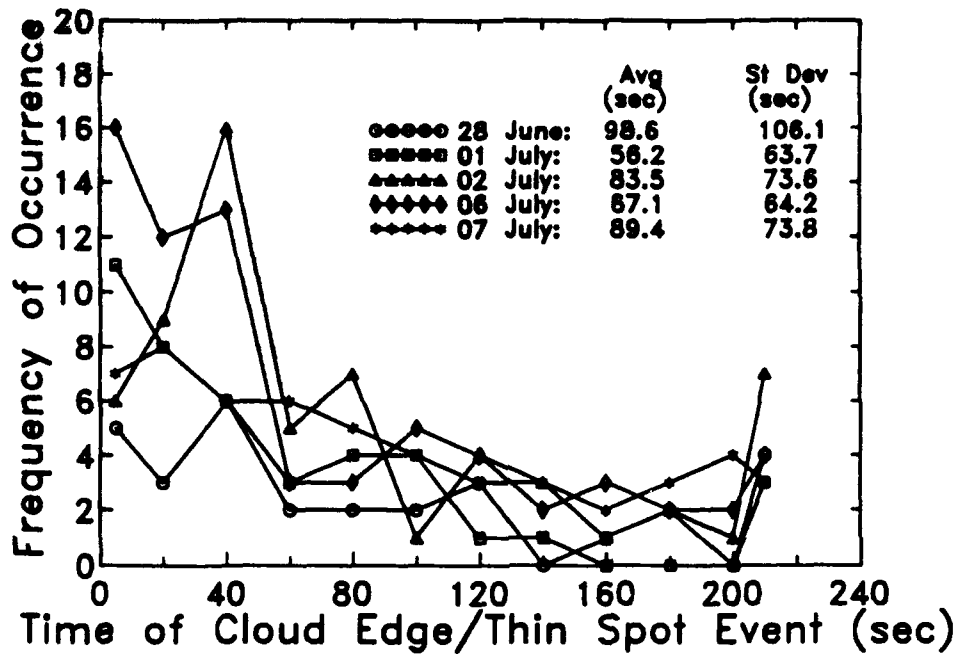


Figure 32. Frequency of Occurrence of Cloud Edges and Thin Spots Events Versus Duration Time. Note that the values for 210 seconds actually represents all occurrences of duration times greater than 210 seconds

4 SUMMARY AND CONCLUSIONS

This report has analyzed solar transmissometer data that were taken during the South Atlantic Backscatter Lidar Experiment (SABLE). There were six days when the instrument was operated: 25 June, 28 June, 1 July, 2 July, 6 July, and 7 July 1989. The instrument was located on Ascension Island, and it measured solar transmission at 532 nm versus time and transmission across the solar spectrum.

Because there were initial concerns about instrument calibration, the first task was to validate the transmission data using the Langley method. Here, the measured solar signals were converted to solar transmissions using calibration factors given by the y intercept on plots of $\sec \phi$ versus $\ln i_{\lambda_s}$ where ϕ and i_{λ_s} are the solar zenith angle and the measured solar signal, respectively. Transmissions derived from the Langley method were 5 to 10% less than those derived from the standard calibration procedure, except for 6 July and 7 July 1989 where there was nearly perfect agreement between the two calibration techniques. The extensive data sets on 6 July and 7 July 1989 may account for the excellent agreement because calibration factors for the Langley method can be obtained with more reliable best fit lines.

Next, the time series of solar transmissometer data at 532 nm were used to study the properties of cirrus and boundary layer stratocumulus clouds that passed in front of the sun while the instrument was working. To do this, it was first necessary to separate and remove aerosol and molecular transmissions from the measured solar transmissions to get the cloud transmissions. The removal technique, which made use of "clear sky" values of solar transmission from LOWTRAN7, performed reasonably well.

For the most part, the data taken on 25 June 1989 were analyzed separately because they were influenced by the presence of cirrus and thin cirrus. A qualitative assessment showed the transmissions through cirrus to be between 0.4 and 0.8, and the cirrus thicknesses were estimated to be between 1.0 and 2.2 km. These estimates were consistent with cirrus observations from aircraft for 25 June 1989.

The remainder of the analysis focused on the properties of stratocumulus cloud edges and thin spots. It was shown that stratocumulus had very similar edge characteristics from day-to-day: there was a uniform distribution of cloud transmission values between about 0.1 and 0.7, and the percentages increase significantly as cloud transmissions increase from 0.7 to 0.9. Also, the number of occurrences of cloud thin spots and edges were compared against total of number of cloud occurrences. Although day-to-day variations existed, the comparisons clearly showed that stratocumulus clouds over Ascension Island often are not opaque, and they frequently transmit partial direct solar radiation. Since stratocumulus clouds often cover broad regions of the marine environment, these findings could be of interest to cloud modeling studies that treat stratocumulus clouds as optically thick, developers of ground-to-space systems in the DoD community, and cloud-free-line-of-sight (CFLOS) studies. Finally, the solar transmissometer data were analyzed as a time series in order to estimate the durations of stratocumulus edge and thin spot events. Here, it was shown that time durations of most cloud edges and thin spot events are less than 200 seconds. The distribution is not gaussian; rather, events of less than 60 seconds occur most frequently, and there is a gradual falloff in the number of occurrences as the time durations become longer.

References

1. Alejandro, S.B., Koenig, G.G., Vaughn, J.M., and Davies, P.H. (1990) "SABLE: A South Atlantic Aerosol Backscatter Measurement Program," *Bul. Am. Meteor. Soc.*, 71:281-287.
2. Hummel, J.R., and Longtin, D.R. (1992) "Catalog of Data and Information from the 1988 SABLE Mission," in progress.
3. Hummel, J.R., and Longtin, D.R. (1992) "Catalog of Data and Information from the 1989 SABLE Mission," in progress.
4. Kneizys, F.X., Shettle, E.P., Abreu, L.W., Chetwynd, J.H., Anderson, G.P., Gallery, W.O., Selby, J.E.A., and Clough, S.A. (1988) "Users Guide to LOWTRAN7," Air Force Geophysics Laboratory, Hanscom AFB, MA, AFGL-TR-88-0177, ADA206773.
5. Mill, J.D. and E.P. Shettle (1983) A Preliminary LOWTRAN Snow Model, AFGL-TR-83-0148, Hanscom AFB, MA, ADA129826.
6. Fenn, R.W., Clough, S.A., Gallery, W.O., Good, R.E., Kneizys, F.X., Mill, J.D., Rothman, L.S., Shettle, E.P., and Volz, F.E., (1985) Optical and Infrared Properties of the Atmosphere, Chapter 18 in *Handbook of Geophysics and the Space Environment*, A.S. Jursa Scientific Ed., Air Force Geophysics Laboratory, Hanscom AFB, MA, AFGL-TR-85-0315, ADA167000.
7. Shettle, E.P. (1989) "Models of Aerosols, Clouds, and Precipitation for Atmospheric Propagation Studies", Proceedings of the AGARD 45th Symposium of the Electromagnetic Wave Propagation Panel on *Atmospheric Propagation in the UV, Visible, IR, and mm-Wave Region and Related System Aspects*, Copenhagen, Denmark, 9-13 October 1989.
8. Allen, C.W. (1973) Astrophysical Quantities, Athlone Press, London.
9. ONTAR Corporation (1986) PCTTRAN, ONTAR Corporation, Brookline, Massachusetts.
10. Christiansen, L. (1979) Spectral Radiometric Measurement and Analysis Program, Volume I, E.K.
11. Lurie, N. (1977) Calibration of PAR317S MRV, E.K.
12. EG&G MRMS Operation Manual, Vol. IV.
13. Christiansen, L. (1976) Memorandum to G. Bouk.

Calibration and Reduction of Solar Transmissometer Data

This appendix describes the standard procedure for calibrating and reducing the solar transmissometer data taken during SABLE 89. Most of material in this appendix is a compilation of notes from PhotoMetrics, Inc., the group responsible for the collection of the data.

Effectively, calibration of the EK/EG&G solar transmissometer is done in two phases. The first part involves the calculation of a nearly invariant ratio of instrument response to the ribbon filament calibration lamp and to solar input. The second part uses wavelength scans of the lamp taken before and after each data recording session (typically morning and evening) to monitor and correct for variations in instrument response during operation. Instrument dark current is recorded before and after each set of measurements (monitor scans or transmission scans) and used to remove the linear drift in the instrument baseline. Differences in the data reduction procedure for SABLE 89 are given at the end of this appendix.

A.1 Solar Power Input to the Transmissometer

The spectral solar power input to the integrating sphere, P_s , is given by

$$P_s = T_A T_o A \int_0^{2\pi} d\Phi \int_0^{\theta_o} B(\theta, \Phi) \sin \theta d\theta \quad (A-1)$$

where T_A is the atmospheric transmittance, T_o is the transmittance of objective lens, A is the area of objective clear aperture, θ_o is the 1/2-angle of telescope field of view (FOV) including the measurement field stop aperture, and $B(\theta, \Phi)$ is the solar radiance within FOV at (θ, Φ) . In this equation, as in most of the treatment that follows, explicit dependence of physical parameters on wavelength, λ , has been suppressed for notational convenience. Assuming that the sun is centered along the optic axis and noting that $\theta_o \ll 1$, Eq. A-1 can be rewritten as

$$P_s = 2\pi\theta_s^2 T_A T_o A \int_0^{\beta_o} B_s(\beta) \beta d\beta \quad (A-2)$$

where θ_s is the 1/2-angle subtended by the solar disk, β is θ/θ_s , and β_o is θ_o/θ_s . Note that β represents the fraction from the center to the edge at which a ray at angle θ strikes the solar disk. The apparent radiance across the solar disk varies because of emission and reabsorption effects in the solar atmosphere. Usually the variable part of the radiance is separated out such that

$$B_s(\beta) = B_s(0)L(\beta) \quad (A-3)$$

where $B_s(0)$ is the radiance at the center of the solar disk and the function L accounts for the observed darkening toward the edge (limb) of the solar disk. This limb darkening exhibits a

significant wavelength dependence which is taken to be implicit. Allen⁸ has given three alternate forms for L as a function of $\mu \equiv \sqrt{(1 - \beta^2)}$. In the present calibration procedure, $L(\mu)$ is given by

$$L(\mu) = 1 - u - v + u\mu + v\mu^2 \quad (A - 4)$$

where the parameters u and v , are given at a set of wavelengths, and interpolation is required when calibrating throughout the bandpass of the transmissometer. Defining the parameter

$$F(\alpha) \equiv \int_0^\alpha L(\beta)\beta d\beta = \int_{\sqrt{1-\alpha^2}}^1 L(\mu)\mu d\mu, \quad (A - 5)$$

the mean solar radiance, \overline{B}_s , and the solar irradiance, I_s , can be written as

$$\overline{B}_s = 2B_s(0)F(1) \quad (A - 6)$$

$$I_s = \overline{B}_s\Omega_s \quad (A - 7)$$

where $\Omega_s = \pi\theta_s^2$ is the solid angle subtended by the solar disk. Using these definitions, Eq. A-2 can be rewritten as

$$P_s = LDF(\beta_o) \frac{T_A T_o A I_s \Omega_o}{\Omega_s} \quad (A - 8)$$

where Ω_o is the solid acceptance angle of the telescope ($\pi\theta_o^2$) and the limb darkening factor, $LDF(\beta_o)$, is

$$LDF(\beta_o) = \frac{\beta_o^{-2} F(\beta_o)}{F(1)}. \quad (A - 9)$$

Note that LDF equals one if the solar disk were uniformly bright. Physically, the LDF is the ratio of the mean radiance of the imaged fraction of the solar disk to that of the entire disk.

⁸ Allen, C.W. (1973) Astrophysical Quantities, Athlone Press, London.

A.2 Calibration Equation

The power input to the integrating sphere from the calibration lamp is

$$P_c = T_o A \Omega_c R_p B_c \quad (A - 10)$$

where Ω_c is the acceptance solid angle of telescope including the calibration field stop aperture, R_p is the reflectance of parabolic mirror in lamp housing, and B_c is the brightness of ribbon filament calibration lamp. Since the detector current is proportional to input power, the ratio of the solar signal current, i_s , to the calibration current, i_c , can be written as

$$\frac{i_s}{i_c} = \frac{P_s}{P_c} = \frac{I_s \Omega_o LDF}{\Omega_c \Omega_s R_p B_c} T_A. \quad (A - 11)$$

Inverting this expression, the atmospheric transmittance is

$$T_A(\lambda) = \frac{K(\lambda)}{i_c(\lambda)} i_s(\lambda). \quad (A - 12)$$

and the calibration ratio, $K(\lambda)$, is defined as

$$K(\lambda) = \frac{\Omega_c \Omega_s R_p(\lambda) B_c(\lambda)}{I_s(\lambda) \Omega_o LDF(\lambda)}. \quad (A - 13)$$

where for emphasis, the wavelength dependences are explicitly noted in Eqs. A-12 and A-13. In Eq. A-12, the dark current baseline is first subtracted from the signal and calibration currents to yield i_{sb} and i_{cb} respectively. The atmospheric transmission then becomes

$$T_A(\lambda) = \frac{K(\lambda)}{i_{cb}(\lambda)} i_{sb}(\lambda) \quad (A - 14)$$

where the factor $K(\lambda)/i_{cb}$ is the calibration expressed as transmission per nano-amp of signal. The following section discusses the physical parameters used to determine $K(\lambda)$.

A.3 Calibration Constant

A.3.1 Solar Parameters

The solar solid angle is taken to be 6.22×10^{-5} str, corresponding to a full cone angle of 0.51° . The solar irradiance outside the Earth's atmosphere is obtained from PCTTRAN6⁹. The annual variation of a few percent, which occurs in both these quantities, should cancel out upon taking the ratio needed in Eq. A-13. Note that I_s/Ω_s is the mean solar radiance which is independent of observation distance. Neither the appropriate Ω_s to use with PCTTRAN6 data nor the absolute accuracy of the PCTTRAN6 data has been determined for calibration, but PhotoMetrics, Inc. has estimated the uncertainties to be less than 3%.

⁹ ONTAR Corporation (1986) PCTTRAN, ONTAR Corporation, Brookline, Massachusetts.

A.3.2 Telescope

The ratio of the calibration to the measurement FOV's can be written entirely in terms of the ratio of the field stop diameters employed:

$$\frac{\Omega_c}{\Omega_o} = \left(\frac{d_c}{d_o}\right)^2. \quad (A-14)$$

Substituting Eq. A-14 into Eq. A-13, the calibration ratio can be expressed as

$$K(\lambda) = \pi\theta_s^2 \left(\frac{d_c}{d_o}\right)^2 \frac{R_p(\lambda)B_c(\lambda)}{I_s(\lambda)LDF(\lambda)}. \quad (A-15)$$

Note that due to the ratioing, the result does not depend on the focal length of the objective lens. The instrument specifications for d_c and d_o come from Christiansen¹⁰:

$$d_c = 0.999 \text{ inches}$$

$$d_o = 0.029 \text{ inches}$$

yielding a FOV ratio of $\Omega_c/\Omega_o = 11.65$. Although the number of significant digits in the ratio is specious, the value 11.65 is used to remain compatible with Christiansen². Judging from the number of significant digits quoted for the diameters, the ratio is assumed to have an uncertainty of about 2%.

A.3.3 Calibration Lamp

The spectral radiance of the ribbon filament lamp, B_c , and reflectance of the parabolic mirror, R_p are taken from Lurie¹¹. For reference, the adopted values for these parameters are shown in Figures A-1 and A-2. The spectral radiance of the lamp was measured by Optronics in September 1974. Although a later recalibration was performed in February 1977, these data are tabulated at fewer wavelengths in Lurie¹¹. The differences between measured spectral radiances from September 1974 and February 1977 are generally less than 2%. For SABLE 89, a larger uncertainty is the use of these calibrations 15 years later. Therefore, without recalibration, the lamp radiance can be trusted to no better than 5%. Also a similar, if not greater, uncertainty is associated with the mirror reflectance which was measured in December 1975.

For calibration throughout the instrument bandpass, mirror reflectances were linearly interpolated from tabulated values in Lurie³ since no model is available. For the lamp radiance, a black body temperature is found by fitting the radiance to the black body spectrum with a linearly varying emissivity. This temperature is then used to interpolate between tabulated values of lamp radiance.

The calibration ratio, $K(\lambda)$, obtained from the above procedure and Eq. A-13 is shown in Figure A-3. Due to the uncertainties mentioned above, a systematic error on the order of 10%

¹⁰ Christiansen, L. (1979) Spectral Radiometric Measurement and Analysis Program, Volume I, E.K.

¹¹ Lurie, N. (1977) Calibration of PAR317S MRV, E.K.

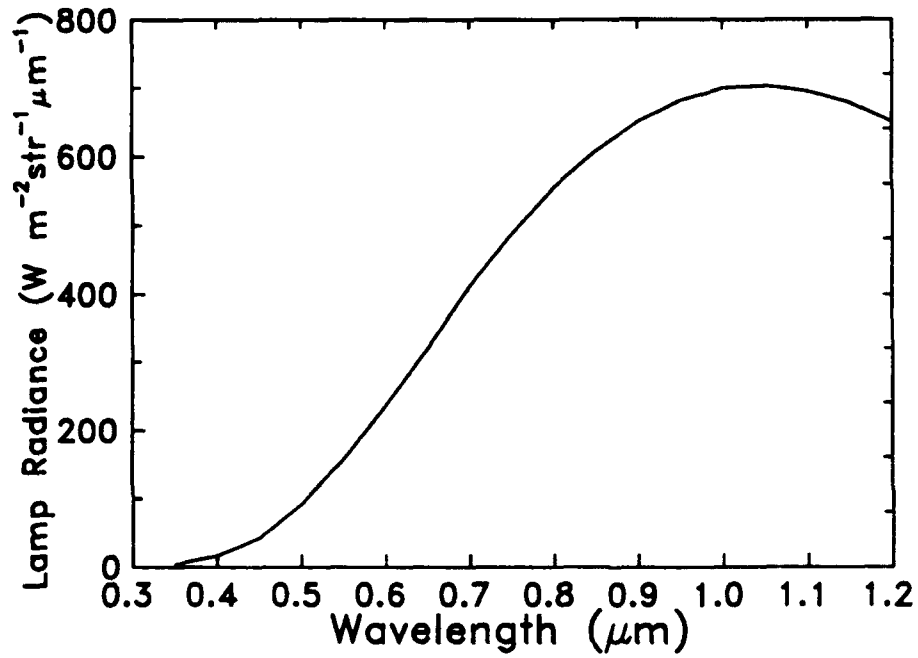


Figure A-1. Spectral Radiance of the Ribbon Filament Lamp, B_c , as a Function of Wavelength

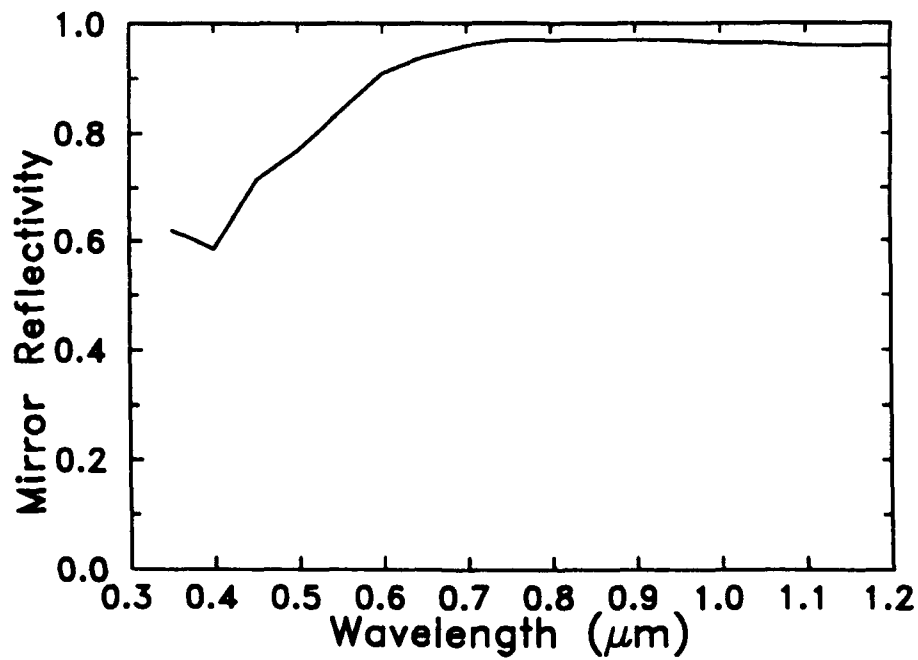


Figure A-2. Spectral Reflectance of the Parabolic Mirror, R_p , as a Function of Wavelength

can be expected in the calculated calibration curve. Most of this error is due to uncertainties in lamp radiance and mirror reflectance. However, the errors involved may be underestimations given the length of time from the last measurement of these quantities.

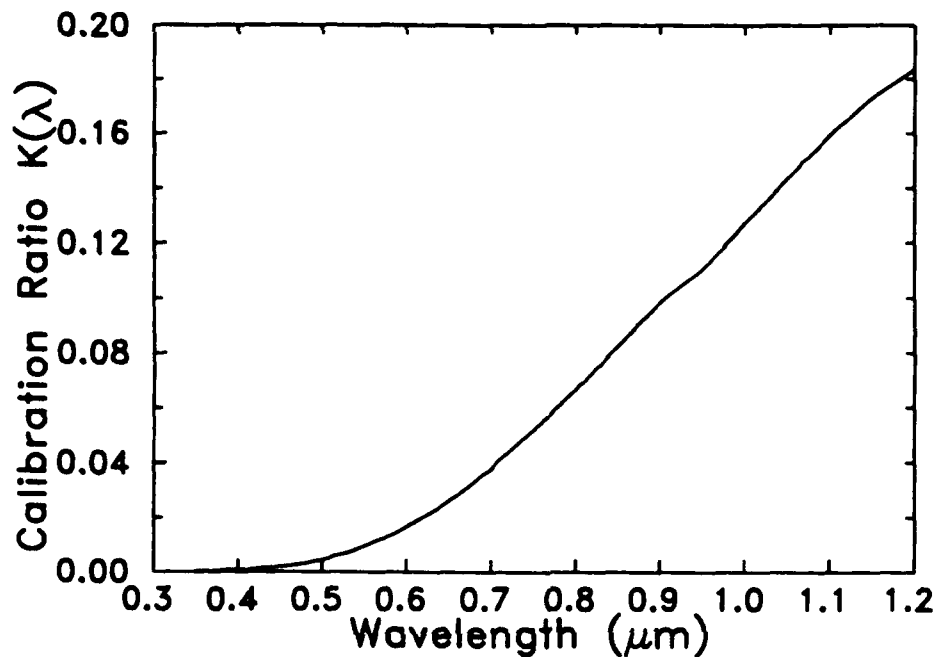


Figure A-3. Calibration Ratio, $K(\lambda)$, for the Solar Transmissometer as a Function of Wavelength

A.4 Measurement Errors of the Signal and Calibration Currents

The two main sources of error in the measurement of the signal, i_s , and calibration currents, i_c , are variations in detector gain and dark current which are discussed below. Also contamination of data below $0.55 \mu\text{m}$ by the reentrant spectrum of longer wavelength radiation is discussed.

A.4.1 Detector Gain

Typically, lamp calibrations (*i.e.*, measurement of i_c) are done before and after all solar data are collected. During this time, gain variations on the order of 10% have been observed. The detector housing has incorporated an LED source and constant current supply so that the gain can be monitored and, if necessary, corrected by trimming the PMT high voltage. This allows for compensation of gain drift to about a 1% level if the internal calibration source is assumed to be repeatable to better than 1%.

A.4.2 Dark Current

Expected signal and calibration currents above about $1\ \mu\text{m}$ and calibration currents below about $0.45\ \mu\text{m}$ are on the order of the detector dark current. Measurement and subtraction of this dark current is necessary in these spectral regions. Due to the age of the detector cooling unit, thermal drifts can cause significant variations in the dark current over a time scale of minutes. Currently, dark currents are measured before and after each series of measurements (e.g., a spectral scan) and dark current values are obtained by means of an interpolation.

A.4.3 Reentrant Spectrum

Recently it was discovered that calibration lamp data, i_c , below about $0.55\ \mu\text{m}$ were significantly contaminated by the reentrant spectrum of light above about $0.7\ \mu\text{m}$. This phenomenon, which is primarily an instrument design problem, occurs when radiation from the calibration lamp enters the Evert-Fastie monochromator with the grating angle set such that light rays less than $0.55\ \mu\text{m}$ reemerge from the exit slit. Allowing for multiple passes, it can be shown that light rays longer than $0.7\ \mu\text{m}$ also arrive at the exit slit. If there is significantly more $0.7\ \mu\text{m}$ light, it can rival that of the primary wavelength even though the reentrant spectrum is not focused on the exit slit.

In the future, reentrant effects will be eliminated or accurately corrected. For the present, it was determined that this spurious component accounts for about half of the detector current, i_c , at $0.45\ \mu\text{m}$. However, this correction should be viewed as no more than a stopgap until more accurate measurements can be made.

A.5 Discussion of Previous EK/EG&G Calibrations

Although calibration data from earlier usages of the transmissometer are not available, Christiansen¹⁰, Lurie¹¹, EG&G¹² and Christiansen¹³ contain discussions of the calibration and other features of the solar transmissometer. The calibration equation is derived in the references^{10,11,13}, for example. Unlike the derivation in this appendix, the other derivations include the effect of limb darkening as an afterthought. Notably and unaccountably, references^{10,11,13} employ the $LDF(\lambda)$ as a multiplying factor in $K(\lambda)$ instead of as a divisor as in Eq. A-13. According to the present values of $LDF(\lambda)$, this would lead to overestimates of 90% in the blue and 20% in the red for the atmospheric transmittance in an otherwise correct analysis.

Concerning the reentrant spectrum, it was recognized in the construction phase of the transmissometer that reentrant effects could be significant.¹² The Jarrel-Ash monochromators were customized to contain a vane at the focal plane of the reentrant rays; however, according to reference¹² "in actual experiments in the laboratory, it became clear that the reentry spectrum is very weak compared to the first order spectrum and can be ignored..." Since the use of the vanes in the reentrant blocking position reduces the instrument throughput by about 50%, it is apparent that they were never employed. If indeed reentrant effects were ignored, and there is no

¹² EG&G MRMS Operation Manual, Vol. IV.

¹³ Christiansen, L. (1976) Memorandum to G. Bouk

indication otherwise, the analysis would underestimate the atmospheric transmission in the blue by a factor of two with little effect at wavelengths above $0.60 \mu\text{m}$. According to PhotoMetrics, Inc., it is interesting to note that this underestimate of transmission in the blue comes close to compensating for the possible overestimate due to misuse of $LDF(\lambda)$ as discussed above.

A.6 Differences in Data Reduction for SABLE 89

SABLE 89 was the first large data set taken with the solar transmissometer. Calibration was only performed once per day, so lamp monitor scans nearest in time to each data set were utilized. Data taken on 25 June and 28 June used the calibration taken on 29 June. To account for reentrant spectra, an estimated correction was applied to the short wavelength data. The assumption was that one half of the light measured at $0.45 \mu\text{m}$ from the calibration lamp was due to multiply reflected light from longer wavelengths and that by $0.80 \mu\text{m}$, there was no reentrance. Values subtracted from the calibration data were as follows:

1. 0.114 between 0.35 and $0.45 \mu\text{m}$.
2. A linearly decreasing ramp to 0.0 at $0.80 \mu\text{m}$.
3. 0.0 between 0.80 and $1.2 \mu\text{m}$.

The value 0.114 was chosen because it was approximately one half of the detector current measured at $0.45 \mu\text{m}$ for the calibration lamp. Below $0.45 \mu\text{m}$ however, the signal due to the calibration lamp is on the order of the detector dark current, and correction between 0.35 and $0.45 \mu\text{m}$ is thus not meaningful (transmissions are also not valid). Also it is noted that from approximately 1.0 to $1.2 \mu\text{m}$, the signal current derived from the calibration lamp is essentially the detector dark current, invalidating transmission measurements in this region.

Data for the eight individual calibrations of SABLE 89 were averaged to obtain the average calibration, $\overline{K(\lambda)}/i_{cb}$. Next the daily calibrations, $C(\lambda)$, were found by normalizing the average calibration to each individual calibration in the wavelength region from 0.85 to $0.87 \mu\text{m}$. Values of atmospheric transmission were then determined from the solar currents, i_s , by subtracting dark current background to get i_{sb} and finding $T_A(\lambda) = C(\lambda)i_{sb}$. For reference, Figure A-4 shows daily calibrations, $C(\lambda)$, for SABLE 89.

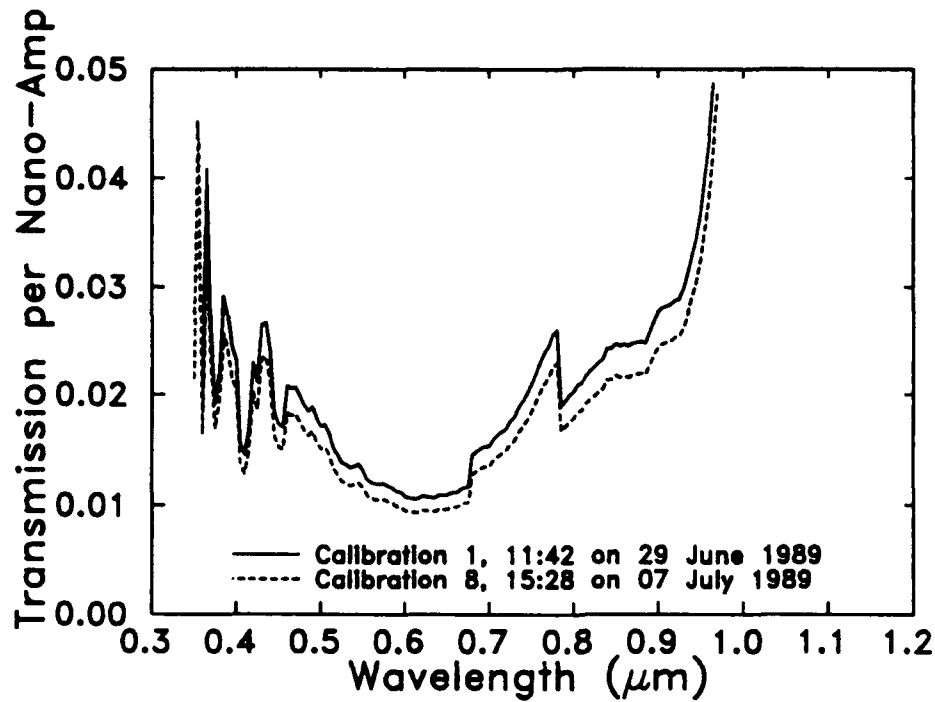


Figure A-4. Daily Calibrations of the Solar Transmissometer as Scaled from the Average for SABLE 89 as a Function of Wavelength. For clarity, only two of the eight calibrations are shown

File Formats and Computer Programs Used in This Analysis

B.1 File Format of the Solar Transmissometer Data

There are 68 files of solar transmission data from SABLE 89, one for each time period when the transmissometer was operated (see Table 1 of the main text). The data are in ASCII format, and the file naming convention consists of a seven digit file name and a *.trn* extension. The first three digits represent the month and day of the measurement, so "628" means 28 June 1989. The second four digits are the start time of the measurement period, so "0631" means the measurement period began at 6:31 Eastern Daylight Time, or 10:31 Local Time for Ascension Island.

Each line of data in a *.trn* file represents an individual solar transmission measurement. Each row of data contains five columns. The meaning of each column is as follows

1. Time in minutes after midnight for Eastern Daylight Time.
2. Wavelength of the measurement in nanometers.
3. Measured solar signal in nanoamperes.
4. Solar tracking parameter.
5. Fractional solar transmission.

For reference, an example of a file containing solar transmission data is shown in Figure B-1.

| | | | | |
|--------|-----|------------|----|------------|
| 463.27 | 531 | 12.604E-01 | 28 | 17.139E-03 |
| 463.33 | 531 | 92.840E-02 | 28 | 12.624E-03 |
| 463.47 | 531 | 41.690E+00 | 15 | 56.689E-02 |
| 463.53 | 531 | 41.390E+00 | 11 | 56.281E-02 |
| 463.60 | 531 | 30.390E+00 | 18 | 41.323E-02 |
| 463.67 | 531 | 26.901E-01 | 28 | 36.579E-03 |
| 463.80 | 531 | 72.400E-01 | 8 | 98.447E-03 |
| 463.87 | 531 | 73.400E-01 | 8 | 99.807E-03 |
| 464.07 | 531 | 34.390E+00 | 15 | 46.762E-02 |
| 464.13 | 531 | 37.990E+00 | 13 | 51.658E-02 |
| . | . | . | . | . |
| . | . | . | . | . |
| . | . | . | . | . |
| . | . | . | . | . |

Figure B-1. Example of a File Containing Solar Transmission Data

B.2 Computer Programs for Data Analysis

During this effort, a number of computer programs were developed to analyze the solar transmission data. All of the computer programs are written with MicroSoft Fortran 5.0. Generally, the computer programs were written in a research framework, in that users must edit some of the hard-wired parameters to suit their needs, and then recompile the code. Brief descriptions of the computer programs are given below. For the most part, the computer programs execute quickly (under a minute or two) on 80286 computer systems.

B.2.1 Program *SIGNALFOR*

This computer program reads files of solar transmission data and then computes the secant of the solar zenith angle and the logarithm of the measured current. This computer program is very useful for determining Langley calibration factors. The input file names are hard-wired into this computer program, and they assume a *.trn* extension. Output from this computer program includes the secant of the solar zenith angle and the logarithm of the measured current. Output is written to files having a *s* appended to the input file names plus a *.dat* extension.

B.2.2 Program *RECALFOR*

This computer program reads files of solar transmission data and then converts the measured currents to transmissions using the Langley method. The input file names are hard-wired into this computer program, and they assume a *.trn* extension. Output from this computer program includes transmissions from the Langley method and the standard calibration procedure, as well as their difference. Output is written to files having the input files name plus a *.dat* extension. Note that appropriate calibration factors for the Langley method must be predetermined (usually from graphical procedures) and then hard-wired into this computer program before it can be used.

B.2.3 Program *REMOVEFOR*

This computer program removes aerosol, molecular, and zenith angle effects from the solar transmission data. The computer program also computes statistical information about the normalized data, such as frequency of occurrence of normalized transmission versus transmission bin, plus averages and standard deviations of cloud thin spots.

Before *REMOVEFOR* can be run, users must decide on a surface visibility to be used to normalize the data. If the surface visibility is not one of those already in the computer program, users must precalculate (using *LOWTRAN7*) an array of space-to-ground transmission at 532 nm versus solar zenith angle for the surface visibility of interest, and then hard-wire them into the program. Users must also add a line of code to perform the interpolation for the desired visibility, and then modify the line of code that actually removes the aerosol and molecular effects. If the surface visibility is already in the program, users must still activate the appropriate line of code for the interpolation, and then modify the line that actually removes the aerosol and molecular effects. Also, the computer program currently calibrates the data using the Langley method, so users must supply an appropriate calibration factor on the line that actually removes the aerosol and molecular effects.

It is important to note that *REMOVE.FOR* will need to be run a few times in order to get the best normalized fit. The general procedure is to run the computer program for a certain surface visibility, plot the results, decide on a better surface visibility, and then try again.

Because the normalization scheme is an iterative process, *REMOVE.FOR* only handles one solar transmissometer data file at a time. The input file name must be hard-wired into the program, and it assumes a *.trn* extension. The normalized data is written to a file having a *n* appended to the input file names plus a *.dat* extension. The statistical information is written to a file named *stats.dat*.

B.2.4 Program *CIRRUS.FOR*

This computer program calculates cirrus transmission in the solar direction versus local time at Ascension Island. Note that the cirrus transmission in the solar direction varies according to a secant of the solar zenith angle relationship. Currently, this computer program determines transmissions for cloud thicknesses between 0.1 km and 2.5 km. The reference values for cirrus transmission are computed with *LOWTRAN7*. There are no input files for this computer program, and the output is written to *cirrus2.dat*.

B.2.5 Program *STRATO.FOR*

This computer program calculates stratocumulus transmission in the solar direction versus local time at Ascension Island. Note that the stratocumulus transmission in the solar direction varies according to a secant of the solar zenith angle relationship. Currently, this computer program determines transmissions for cloud thicknesses between 1 m and 100 m. The reference values for stratocumulus transmission were computed with *LOWTRAN7*. There are no input files for this program, and the output is written to *strcu2.dat*.

B.2.6 Program *TGAPS.FOR*

This computer program reads a file of normalized transmission data, and then identifies time periods of cloud thin spot events. The computer program also performs statistical study on the duration of thin spot events, including frequency of occurrence of thin spot events versus time bin, plus averages and standard deviations of cloud thin spots events.

TGAPS.FOR identifies individual cloud thin spot events by individually examining each normalized data point to see if it is part of a thin spot event. To do this, the normalized data point to be studied is categorized as being cloudy (*i.e.*, $\tau < 0.1$), thin (*i.e.*, $0.1 \leq \tau \leq 0.9$), or clear (*i.e.*, $\tau > 0.9$). If the normalized point being studied is cloudy, the computer program then searches on each side for the closest thin spot or clear point. If the normalized point being studied is clear, the computer program then searches on each side for the closest thin spot or cloudy point. The resulting time difference is then calculated and if it is less than 60 seconds, the normalized point being studied is part of a cloud thin spot event. Note that thin points are always part of a thin spot event.

Currently, *TGAPS.FOR* only handles one normalized data file at a time. Note that the input file for this computer program is the output file from the *REMOVE.FOR* computer program. The input file name is hard-wired into the computer program with a *n.dat* extension. The output from the computer program lists all times and the corresponding normalized transmissions for all gap

events in sequential order. The output is written to a file in which a *g.dat* extension replaces the *n.dat* extension. The statistical information is written to a file named *gap.dat*.